Article:
Stringer, C.D., Carrivick, J.L., Quincey, D.J. et al. (2 more authors) (Accepted: 2025) Land cover change across the major proglacial regions of the sub-Antarctic islands, Antarctic Peninsula and McMurdo Dry Valleys, during the 21st century. Arctic, Antarctic, and Alpine Research. ISSN 1523-0430 (In Press)

Land cover change across the major proglacial regions of the sub-Antarctic islands, Antarctic Peninsula and McMurdo Dry Valleys, during the 21st century

Christopher D. Stringer[1,2], Jonathan L. Carrivick[2], Duncan J. Quincey[2] , Daniel Nývlt[3], Alexis Comber[2]
[1] School of Built Environment, Engineering and Computing, Leeds Beckett University, Leeds, UK
[2]School of Geography and water@leeds, University of Leeds, Woodhouse Lane, Leeds, West Yorkshire LS2 9JT, UK
[3]Polar-Geo-Lab, Department of Geography, Faculty of Science, Masaryk University, Kotlářská 2, CZ-611 37 Brno, Czech Republic

Correspondence to: Christopher D. Stringer (C.D.Stringer@leedsbeckett.ac.uk)

Abstract. Land cover information is essential for understanding Earth surface processes and ecosystems. Here, we use K-means clustering to classify Landsat-8 (OLI) images covering six proglacial sites of sub-Antarctic islands, the Antarctic Peninsula and the McMurdo Dry Valleys at 30 m resolution. We quantify spatial patterns of water, bedrock, vegetation and sediments, to an accuracy of 77 %. Vegetation is most abundant on South Georgia (7 % of the proglacial area) and the South Shetland Islands (1 to 2 %). Furthermore, we use change vector analysis (CVA) to discriminate landcover change in the 21st century. A latitudinal pattern is evident in ice loss and proglacial landscape change; e.g., loss of ice on South Georgia and proglacial landcover change is two orders of magnitude greater than in the McMurdo Dry Valleys. Four of the studied sites had similar landscape stability (64 to 68 % unchanged), with Alexander Island an exception (50 % change) due to recent enhanced glacier melt. Overall, we show how landcover of proglacial regions of the climatically-sensitive sub-Antarctic and Antarctica has changed since 2000, with a CVA accuracy of 80 %. These findings inform understanding of geomorphological activity, and sediment and nutrient fluxes and hence terrestrial and marine ecosystems.

1. Introduction

Consistent land cover information is essential to furthering our understanding of terrestrial environments, ecological niches and the atmosphere, especially across sensitive regions of Earth (Raup et al., 2007; Ban et al., 2015; Chen et al., 2019; Gong et al., 2020). Additionally, land cover maps are a critical resource required to support the research of climate change: particularly those that include information on vegetation coverage (Bojinski et al., 2014). Different types of land cover can change or respond to climatic forcing in different ways, depending on their physical and chemical properties (GCOS, 2010). Owing to the frequent return period and extensive areas covered by satellite images, land cover maps are increasingly being produced using remote-sensing techniques and the changes occurring in the landscape can thus be detected and quantified (Friedl et al., 2010; Lea, 2018; Brown et al., 2022). Several global land cover products have been released in recent years (e.g. (Brown et al., 2022) but they typically do not include Antarctica or sub-Antarctic Islands (e.g. South Georgia), leaving a gap in our understanding of Earth's southernmost continent.

The majority (99.8 %) of Antarctica is covered by ice, with the remaining 0.2 % characterised as nunataks (i.e. mountain peaks that penetrate the ice sheet) or as proglacial regions (Burton-Johnson et al., 2016) (Fig. 1). Proglacial regions are predominantly shaped by the interplay of meltwater from glaciers, which erodes, transports and deposits sediment, and hillslope activity, which largely acts to supply new sediment into the system during mass transport events. In a warming climate, the activity of water and increased mass movements result in greater sediment discharge (Ballantyne, 2008; Staines et al., 2015; Klaar et al., 2015). In polar regions, where permafrost can be extensive, the active layer is an additional and important water and sediment source on days when ground temperatures exceed 0 °C (Humlum et al., 2003; Kavan et al., 2017; Costa et al., 2018; Łepkowska and Stachnik, 2018). All of these factors mean that the Antarctic landscape is highly dynamic.

Maps of land cover and land cover change are particularly important for Antarctica, owing to its dynamic landscape and rapid environmental change (Davies et al., 2013). Unlike most other regions on Earth, human activities are not the major control on land cover type in Antarctica, and the footprint of anthropogenic activities is limited to relatively small areas (Tejedo et al., 2016; Tejedo et al., 2022). Until the start of the 21st century, the Antarctic Peninsula Region (APR) was one of the most rapidly warming places on Earth with a temperature rise of 1.5 °C observed since the 1950s (Vaughan et al., 2003; Mulvaney et al., 2012; Oliva et al., 2017). Following a hiatus in warming at the start of the 21st century, there is evidence that this trend has resumed (Carrasco et al., 2021) and glaciers have continued to respond to the temperature increases of the 20th century and subsequent warming since 2015 (Oliva et al., 2017; Engel et al., 2023). Consequently, glacier mass loss has occurred at an enhanced rate, particularly around smaller ice masses in the APR and sub-Antarctic islands (Oliva et al., 2017; Engel et al., 2018; Rosa et al., 2020). This ice mass loss has resulted in the enlargement of proglacial regions, and they will continue to expand as both land and marine-terminating glaciers continue to retreat with a warming climate (Nedbalová et al., 2013; Lee et al., 2017; Roman et al., 2019).

In this study we will map the land cover of six major proglacial regions in Antarctica: **i)** South Georgia; **ii)** southern Livingston Island and Snow Island (hereafter referred to as Byers Peninsula); **iii)** Deception Island; **iv)** James Ross Archipelago; **v)** Alexander Island, and; **vi)** the McMurdo Dry Valleys (Fig.1). These sites are conspicuous for their lack of consistent land cover data between the sites. Whilst geological and geomorphological studies have produced maps at the sites (e.g. Table 1), they lack a common nomenclature. Similarly, many of these maps are several decades old, or no map of their surface exists. On Alexander Island, for example, there are very few descriptions of the landscape or land cover are available, with limited descriptive accounts (Heywood et al., 1977) and only very limited geomorphology maps of the region available (Salvatore, 2001). In contrast, some regions have been the subject of extensive mapping studies. James Ross Island, for example, has been home to several geological and geomorphological surveys, though these studies are either limited to the Ulu Peninsula (Davies et al., 2012; Mlčoch et al., 2020; Jennings et al., 2021), or lack detail on land cover information beyond the geology (Smellie, 2013). Whilst there have been recent, substantial, efforts in improving the understanding of vegetation extent in Antarctica (Walshaw et al., 2024), there continues to be a lack of understanding of other import land features.

Understanding the make-up of Antarctica's proglacial regions, and how those land surface components are changing, is important because they are a source of water, sediment and solutes. The quantity and spatio-temporal pattern of sediment discharged from Antarctica has profound effects on the ecosystem of the Southern Ocean and polar lakes, which in turn can affect the rate at which carbon is sequestered from the atmosphere (Brussaard et al., 2008; Maat et al., 2019). Additionally, changes in vegetation cover can have wide-ranging impacts on wildlife. In a warming climate, the natural range of indigenous species may increase (Convey and Smith, 2007). Similarly, people visiting the APR and sub-Antarctic may introduce invasive species (Galera et al., 2021; Tejedo et al., 2022). The establishment of invasive species can expand the vegetated area, displace indigenous biota, increase competition and alter food web linkages, potentially threatening the survival of indigenous species (Molina-Montenegro et al., 2012; Hughes et al., 2020). It is, therefore, important to have a baseline dataset that describes the land cover composition of proglacial landscapes (Carrivick et al., 2018; Carrivick et al., 2019) so that future changes may be quantified. Furthermore, understanding how proglacial landscapes have responded to recent ecological and climatic change is also useful for understanding how these systems may evolve in the future (Wilkes et al., 2023).

The aims of this paper are: **i)** to produce the first unified map of land cover across the major proglacial areas of APR, sub-Antarctic and the Dry Valleys; **ii)** to quantify the overall accuracy of our data and how that accuracy varies spatially, and; **iii)** to identify regions that have changed during the 21st century.

1.1 Study Sites

There is a dearth of literature that seeks to characterise proglacial regions, particularly in Antarctica. Some research has been conducted on individual rivers and catchments, notably on the Onyx River ((Chinn and Mason, 2016), James Ross Island's Ulu Peninsula (Davies et al., 2013; Nedbalová et al., 2013; Kavan et al., 2017; Sroková and Nývlt, 2021; Jennings et al., 2021; Kavan, 2021), and on other sub-Antarctic islands, such as the South Shetland Islands (Mink et al., 2014; Oliva et al., 2016). However, these studies have taken varying approaches to characterising landscape compositions, and there is little in way of a consistent land cover dataset of these proglacial regions. Additionally, important global datasets fail to characterise the land cover of Antarctica (e.g. Brown et al., 2022).

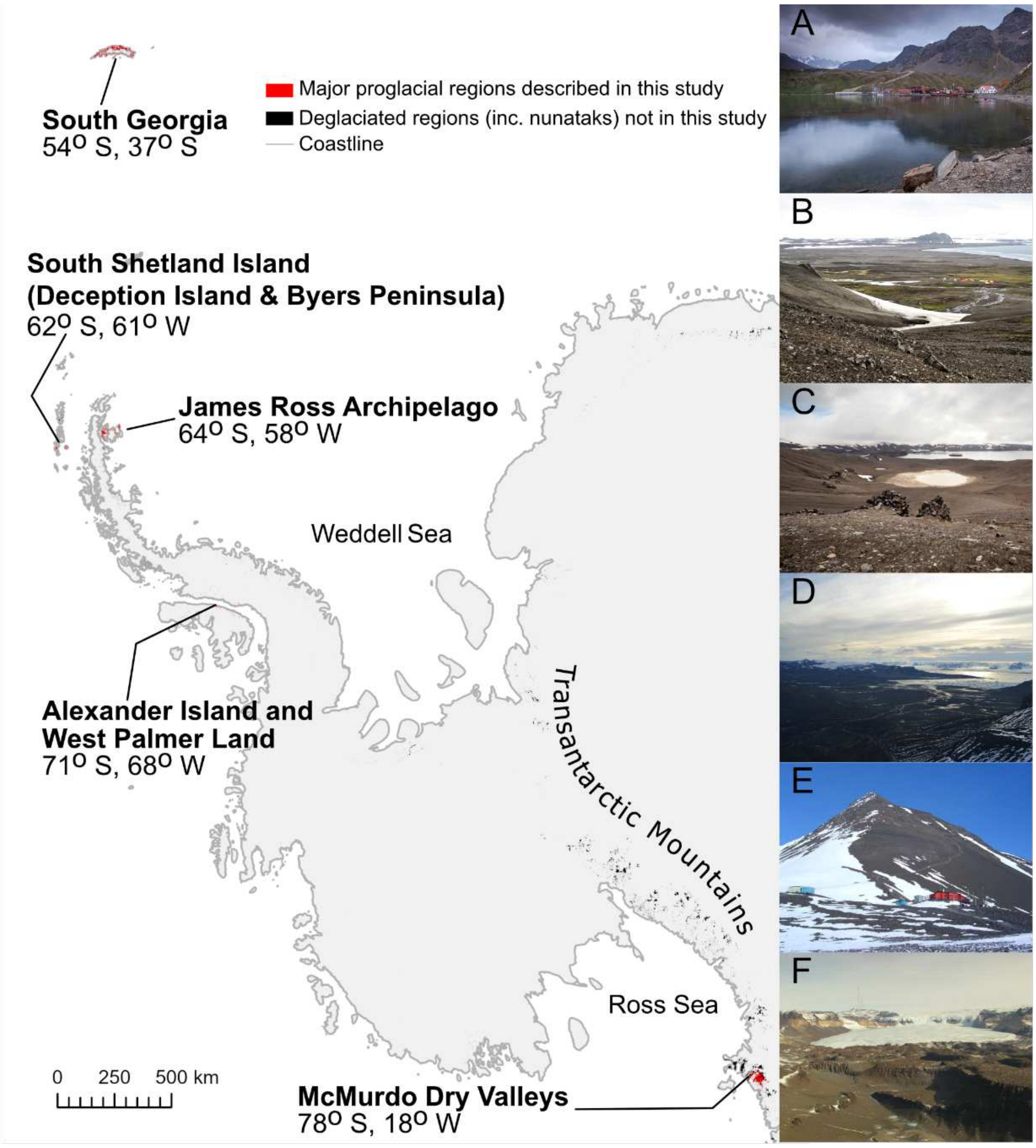

Figure 1: Location of our study sites. The areas analysed have been highlighted in red and span a latitudinal gradient from 54ºS to78ºS . Proglacial regions not analysed in this study have been highlighted in black (Burton-Johnson et al., 2016)and are primarily mountains (e.g. Transantarctic Mountains) or are frequently covered by extensive cloud-cover (e.g. King George Island).

Inset photos A,B,D,E, and F are sourced from Wikimedia Commons. Photos C is by CS. They show: A) Grytviken on South Georgia. Taken in 2009 by Simon Murgatroyd (CC BY-SA 2.0); B) Camp Byers on South Beach (ESP) on Byers Peninsula. Taken in 2017 by "Inoceramid bivalves" (CC BY-SA 4.0); C) Telefon Bay (background), as viewed from the rim of a crater on Deception Island. Taken in 2020 by Espen Mills (CC BY-SA 4.0); D) Abernethy Flats on James Ross Island's Ulu Peninsula, as viewed from Lachman Crags, above Triangular Glacier (looking West), taken in 2022; E) The central station of Fossil Bluff on Alexander Island in 2003. Photo taken in 2003 by "Apacheeng lead" (Public Domain); F) The Wright Valley of the McMurdo Dry Valleys (looking west towards Wright Upper Glacier) in 2013, taken by "Turkish D." (CC BY-SA 4.0).

1.1.1 Climate

All of the six study sites have polar climates but span both maritime and continental settings. The sites are positioned along a latitudinal gradient and so permit an analysis of land cover variability with climatic patterns. The most northern site, South Georgia, is characterised by its high relief and has a mean annual air temperature (MAAT) of 3 °C, as well as receiving over 2000 mm of precipitation per year (Strother et al., 2015; Bannister and King, 2015). Over half of South Georgia is glacierised (Bannister and King, 2015). The South Shetland Islands are characterised by a polar maritime climate, with air temperatures regularly exceeding 0 °C in summer. The humid environment, due to its maritime location, ice-free seas and regular cyclonic activity, results in liquid precipitation falling regularly in the summer months (Bañón et al., 2013). The James Ross Archipelago, to the north-east of the Antarctic Peninsula, has a MAAT of -7 °C and has a semi-arid polar continental climate (Kaplan Pastíriková et al., 2023). The two more southerly sites; Alexander Island and The McMurdo Dry Valleys, have continental climates (Harangozo et al., 1997). Alexander Island, specifically Fossil Bluff, has a MAAT of -9 °C and receives approximately 200 mm of precipitation each year (Harangozo et al., 1997; Davies et al., 2017). The McMurdo Dry Valleys are distinctly colder and drier than the other sites; they are hyper-arid due to katabatic winds and have a MAAT of -17 °C to -20 °C (Doran et al., 1994; Marchant and Head, 2007).

2. Methodology

2.1. Site Selection

Our site selection was informed by the British Antarctic Survey's (BAS) rock outcrop datasets (Burton-Johnson et al., 2016; Gerrish et al., 2020), allowing us to focus primarily on the non-glacierised landscape. Nunataks in the interior of the ice sheets were excluded because they were too small to classify at 30 m resolution, and we could assume their classification to be bedrock. Since they are disconnected from the coastline, they can also be assumed largely unimportant as sediment sources to the Southern Ocean. Fossil Bluff and other coastal regions in Alexander Island and Palmer Land were included and are interesting for their proximity to George VI Sound. These regions may become important sediment sources in the near future, as exceptional melting in this region appears to have increased the likelihood of the George VI ice shelf collapsing (Banwell et al., 2021). We further narrowed the site choices to consider only those regions with cloud-free Landsat-8 Operational Land Imager (OLI) images.

2.2. Land cover classifications

In the last decade, satellite data from the Landsat and Sentinel programmes have become open source and increasingly easy to access. In tandem with improved computational power, such as that provided by cloud-based platforms like Google Earth Engine (GEE), it is now possible to produce land cover maps at a medium spatial resolution (10 m to 30 m) using openly available data. The Landsat-8 satellite also has the benefit of being part of a continuation program, making inter-decadal comparison possible.

2.2.1. Image selection and pre-processing

We classified Landsat-8 OLI (Operational Land Imager, top-of-atmosphere, TOA) images acquired between 2016 and 2020 (see supplementary material section 1.6 for details) in GEE and ESRI ArcGIS Pro 2.6.0 (ArcPro), primarily using K-means clustering (using GEE's default settings, including 10 randomised seeds). While we have chosen to use GEE and ArcPro for this research, it would be functionally possible to repeat our methodology in other software. We chose Landsat imagery, rather than higher-resolution images (such as Sentinel-2), because of its extensive archive dating back to 1972. Suitable images had low cloud cover (less than 20 % over land) and limited snow cover. Images were cloud masked (using Landsat's quality

assessment band) and, where more than one image was available, we mosaicked them, taking the least cloudy/snowy scene as the uppermost image, thus minimising the snow and cloud cover across the unified scene.
To ensure consistency with older Landsat images, we only selected six bands representing the visible and infrared wavelengths (red, green, blue, near-infrared, shortwave infrared 1, and shortwave infrared 2, ranging from 0.45 to 2.29 µm) from the images for classification. We added three further bands to the image in the form of the normalised difference snow index (NDSI, Eq. 1), the normalised difference vegetation index (NDVI, Eq. 2), and the normalised difference water index (NDWI, Eq. 3). These aided the classifier in the identification of key land cover classes (ice, vegetation, and water, respectively).

$$NDSI = \frac{green - swir1}{green + swir1} \tag{1}$$

$$NDVI = \frac{nir - red}{nir + red} \tag{2}$$

$$NDWI = \frac{green - nir}{green + nir} \tag{3}$$

Where:

- green = band 3 of Landsat 8 OLI, wavelength (λ) = 0.53–0.59 µm
- swir1 = shortwave infrared 1, band 6, λ = 1.57–1.65 µm
- red = band 4, λ = 0.64–0.67 µm
- nir = near-infrared, band 5, λ = 0.85–0.88 µm

We clipped the images to a 1 km buffer around their coastline (Gerrish, L., Fretwell, P., & Cooper, 2021) and topographically corrected them to adjust for the effect of relief on the illumination of images using the Sun Canopy Sensor + C method (Soenen et al., 2005) with the REMA DSM (Reference Elevation Model of Antarctica Mosaic Digital Surface Model) (Howat et al., 2019) at 30m resolution (equivalent to the resolution of Landsat-8 OLI multispectral bands). South Georgia, which is not covered by REMA, was corrected using the SRTM DEM (Shuttle Radar Topography Mission Digital Elevation Model), also at 30m resolution (Farr et al., 2007). Subsequently, we conducted a principal component analysis of the images, and the first three components, containing 99.6 % (± 0.3 %) of the data, were selected for classification (Frohn et al., 2009; Chasmer et al., 2020).

2.2.2. Classification

We used a hierarchical K-means clustering approach to classify Landsat-8 (OLI) images (**Figure 2**). K-means is widely used in land classification studies (Grimes et al., 2024; Phiri and Morgenroth, 2017), and is preferential to over other unsupervised approaches (e.g. ISODATA) since it can be used to identify a user-defined number of classes. K-means works by segmenting an image into distinct clusters, which the user then interprets to classify these clusters using existing knowledge of the field, or previously published maps often based on field research (e.g. Table 1). A first-order land classification (clustered with K = 75, see supplementary material section 1.1) of "land", "snow & ice" (hereafter referred to simply as "ice"), and "water" informed the subdivision of each of these classes in a second, more detailed, analysis of the dominant land cover classes (further details in supplementary material section 1.2.). A two-stage approach was used to limit misclassification by ensuring water, ice, and bare land were in distinct classes. The code used to produce this classification is also publicly available (see section 2.4.5).

We used this first-order land classification to subset each image accordingly and then to cluster these resulting images into 40 discrete groups (K = 40). Specific K values were determined through expert judgement and represent values that minimised the chance of misclassification (see further details in supplementary material 1.1). Using the limited catalogue of published maps and literature available for these areas (see Table 1); we visually inspected these clusters to manually assign each of them a final land classification. Our first-order land class was subset into five classes “Bedrock”, “Coarse/wet sediment”, “Fine & dry sediment”, “Vegetation”, and “Land (non-differentiated)”. The water class subset into “Water” and “Turbid water”, while the ice class subset into “Ice” and “Wet ice”. In cases where clouds partially obscured land, we assigned pixels to the more general class of “Land (non-differentiated)”. Therefore, we produced ten land classes that describe eight distinct surface types (plus no data and land undifferentiated, see supplementary material for more details), that could be identified from a combination of field observations and a review of available maps of Antarctica (**Table 1**) and finding commonalities between them (further details in supplementary material section 1.3.).

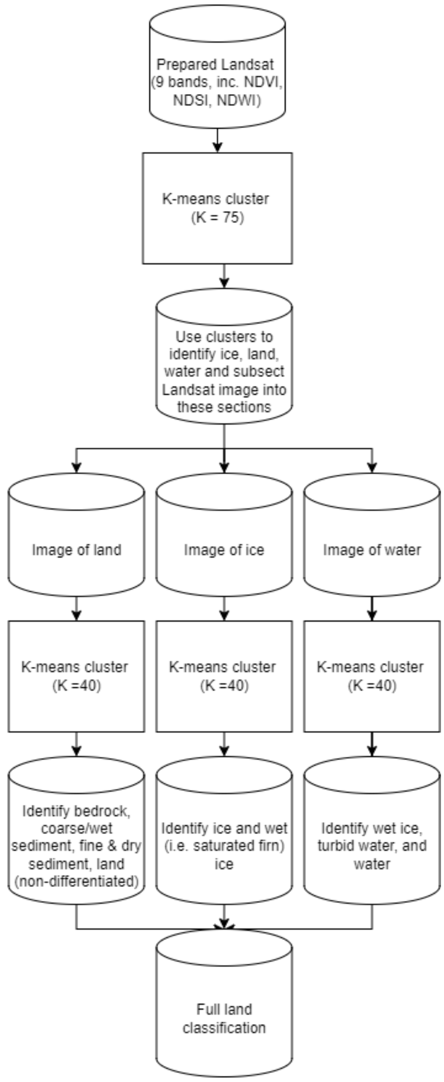

Figure 2: Our approach to classifying land cover

During the classification process, we created two different sedimentary classes because we found that pixels containing wet sediments (such as rivers) or blocky superficial sediments, such as scree, clustered distinctly from those pixels that contain sediments smaller than cobbles in size and fissile sedimentary rocks. This approximate grain size threshold was derived from information on geomorphological maps for the region (Jennings et al., 2021), and observations made on James Ross Island during the 2022 field season. We emphasise that the first of these two classes describe pixels that contain sediment that may be coarse, wet, or both. The second of these classes describes surfaces with fine sediments with minimal water content.

Table 1: Resources used to interpret clusters and assign them to a land class

Location	Resources
James Ross Island	Geomorphology map, Jennings et al. (2021) Geomorphology map, Davies et al. (2013) Geological map, British Antarctic Survey, Smellie et al. (2013) Geological map, Czech Geological Survey, Mlčoch et al. (2020) Vegetation map, (Barták et al., 2015))
Dry Valleys	Interactive geological map, SCAR, (Cox et al., 2023)
Alexander Island	Geological map, British Antarctic Survey (1981)
Deception Island	Geology and geomorphology Map , British Antarctic Survey, Smellie et al. (2002) ASPA 140 (map of vegetation), (Secretariat of the Antarctic Treaty, 2022)

Livingston Island	Geomorphology map, Lopez-Martinez et al. (1996) Vegetation map, Ruiz-Fernández et al. (2017)
South Georgia	Geomorphology map, Clapperton (1971)

2.3. Accuracy Assessment

Having used the limited pre-existing maps and field-survey data to inform our interpretation of the K-means clusters, we had to depend on finer-resolution imagery as the primary independent validation source, with interpretations of images aided by the use of previously published maps. Although we could not find alternative land cover data, we still used the methods of best practice described by (Olofsson et al., 2013, 2014) to ensure our accuracy assessment was robust (see supplementary material section 1.5). Therefore, we generated 3000 random points, stratified by the area of each land class, and visually compared them to 10 m resolution Sentinel-2 MultiSpectral Instrument (MSI) images. Sentinel-2 MSI images were used as an independent data source for validation as they are finer resolution than Landsat images, thus giving a better indication of the "true" land cover. Given the dominance of the ice class in our classification, this meant most of the stratified sample points landed on ice. We conducted a second level of accuracy assessment with 1000 points on just the proglacial classes to ensure their accuracy was adequately calculated.

The classes of turbid water and wet ice were particularly problematic because they typically comprised episodic sediment plumes and snow/ice melt. Therefore, we combined these classes with water and ice respectively for the purposes of accuracy assessment. We produced a 10 km resolution grid to display the spatial variability in the accuracy of this classification (as a proxy for confidence), with each cell colour-coded according to the percentage of accurate assessment points within it. Full accuracy assessment matrices are available in the supplementary material (section 1.5).

We also compared the spectra for each land-type, to ensure each land-type could reasonably be differentiated from each other.

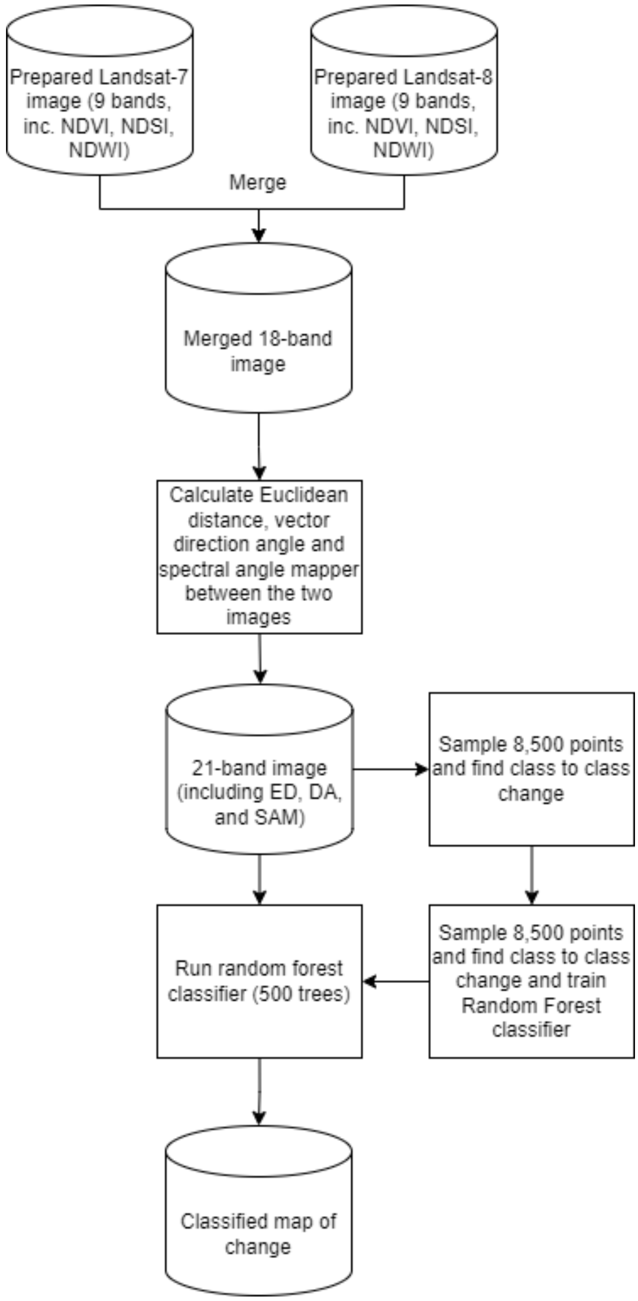

Figure 3: The change detection (CVA) approach used in this study

2.4. Change detection

We repeated the search described in section 2.2.2 for Landsat 7 Enhanced Thematic Mapper Plus (ETM+) images acquired for each of our sites between 2000 and 2003 and conducted change detection (**Fig 3**). This search resulted in a pair of image mosaics (hereafter referred to as image pairs) for five sites, comprising a mosaic from the early 2000s (Landsat-7), and a mosaic from close to 2020 (Landsat-8). It was not possible to find a suitable image for Deception Island, so we could not conduct change detection for this site; this meant change detection was conducted over only five of the six sites for which a land cover map was produced. We manually inspected the image pairs for each site to ensure they were co-registered using GIS. We aimed to ensure that both mosaics comprised images collected from the same time of year, to ensure they represent the same part of the growth and hydrological season, and avoided images with high snow cover, where possible. In some cases, poor image availability meant that some image pairs could not be collected from the same time of the year (though the temporal difference was minimised). We ensured that key features such as flowing rivers and unfrozen lakes, were, as much as possible, present in both mosaics. Then we conducted a change vector analysis (CVA) to identify regions of change in each of our sites, using the approach described by (Xu et al., 2018). Further details of the CVA approach used can be found in the supplementary material (section 1.4).

Table 2: Class to class changes and their abbreviations

Class to class change	Abbreviation
Wet ice to coarse/wet sediment	WITC
Ice to fine & dry sediment	ITF
Ice to coarse/wet sediment	ITC
Ice to turbid water	ITT
Coarse/wet sediment to turbid water	CTT
Coarse/wet sediment to wet ice	CTWI
Fine & dry sediment to bedrock	FTB
Coarse/wet sediment to bedrock	CTB
Coarse/wet sediment to fine & dry sediment	CTF
Coarse/wet sediment to vegetation	CTV
Bedrock to coarse/wet sediment	BTC
Fine & dry sediment to coarse/wet sediment	FTC

2.4.2. Accuracy assessment

To validate the accuracy of our change maps, we reproduced the change detection analysis on Byers Peninsula with a 70/30 split of the training points between the classifier and validation. This approach is regularly used to assess the accuracy of land cover and change products, in the absence of independent data (Xu et al., 2018), and this ratio between training and validation has been shown to be most reliable (Adelabu et al., 2015). By splitting the data 70/30 between training and validation, the 30 % of pixels used for validation are "independent" of those used by the classifier. To ensure this split was unbiased, we randomly sorted the training points.

2.4.5 Code availability

The codes used in these methods are available at:

Christopher D Stringer. (2022). Contemporary (2016–2020) land cover across West Antarctica and the McMurdo Dry Valleys [Code] (Version 1). Zenodo. https://doi.org/10.5281/zenodo.6720051 ; and:

Christopher D Stringer. (2023). 21st century land cover change across the major proglacial regions of West Antarctica and the McMurdo Dry Valleys [Code]. (Version v1). Zenodo. https://doi.org/10.5281/zenodo.7991208

3. Results and interpretations

3.1. Land cover classifications

3.1.1. The land classes

The largest land class at our sites is ice; the large ice sheets and glaciers at all sites have been mapped, though this class also includes limited snow cover. While mapping ice masses is not the primary goal of this study, the high accuracy (see section 3.3.1) of the ice class makes this dataset a useful resource to assess changes in the small, land-terminating glaciers within our study sites (Fig. 4).

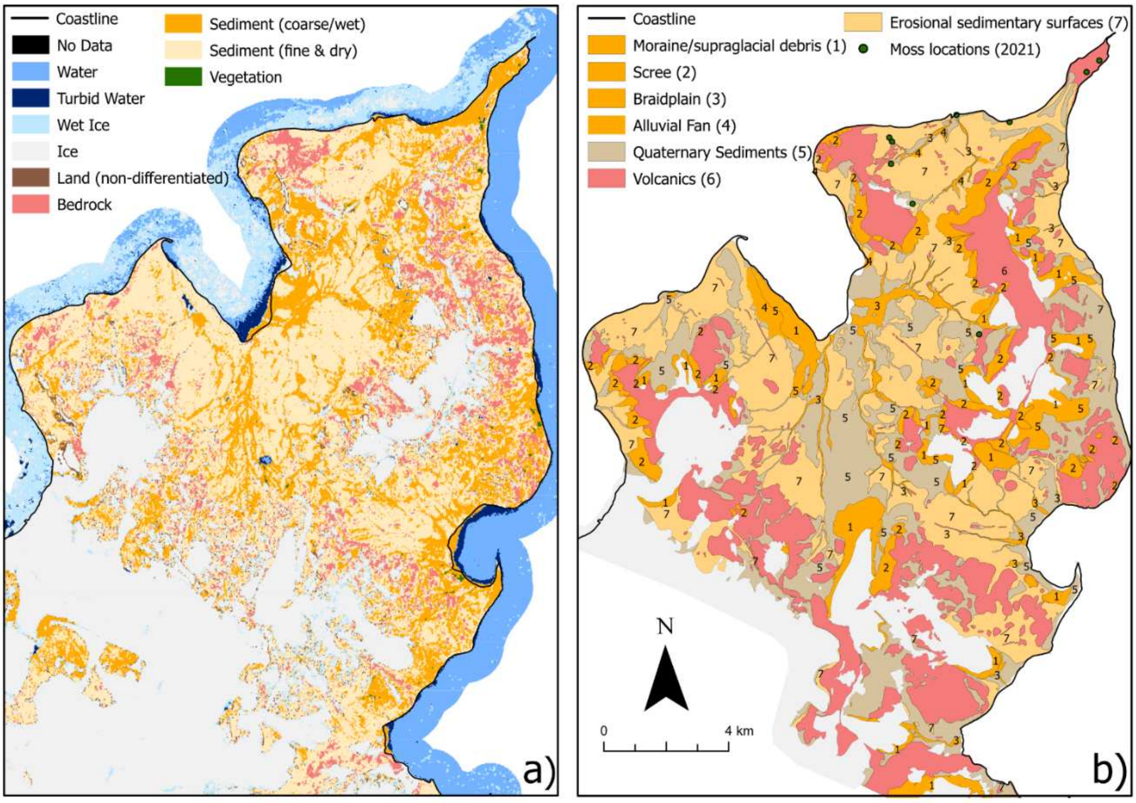

Figure 4: A comparison between , a) the land classification produced in this study; b) a geomorphology map, adapted from Jennings et al. (2021). Jennings et al. (2021) produced this data through a series of extensive field surveys on the Ulu Peninsula. Vegetation locations as collected in the field by Jan Kavan (of CARP) in 2021 are also displayed. Note the similarities in the ice class, locations of river systems, and scree slopes. NB: the colours in panel b have been adapted to allow a more direct comparison with the map produced in this study (a).

Of the sedimentary classes, coarse and wet sediment is the predominant land class at four of the six sites, particularly on South Georgia and Byers Peninsula, where it represents the majority (57 % and 56 % respectively) of the proglacial land cover (Fig. 6). This land class includes the major surface drainage networks of Antarctica (Fig. 4) for example, it accurately depicts the major rivers of the Bohemian Stream and Abernethy River on James Ross Island and the Onyx River in the McMurdo Dry Valleys (c.f. (Chinn and Mason, 2016; Kavan et al., 2017; Jennings et al., 2021). The coverage of fine and dry sediment class varies inversely to that of the coarse/wet sediment. For example, on South Georgia, the 57 % coverage of coarse sediment is in comparison to a 33 % coverage of fine and dry sediment. On Deception Island, where fine and dry sediments are the dominant land class (53 %), there is only 26 % coverage of coarse/wet sediment (Fig. 6). At all of the sites, between 70 % and 80 % of the proglacial surface is covered by sediment. The bedrock class, which primarily describes igneous and metamorphic rock surfaces, is most abundant on Deception Island, comprising 14 % of its proglacial areas (Fig. 6). It is of similar abundance in the Dry Valleys (13 %), with between 7 and 9 % of Alexander Island, James Ross Archipelago, and Byers Peninsula comprised of bedrock. The absence of the bedrock class on South Georgia is accounted for by its lack of igneous outcrops, as well as well-developed sedimentary systems and extensive vegetation cover (Clapperton, 1971)

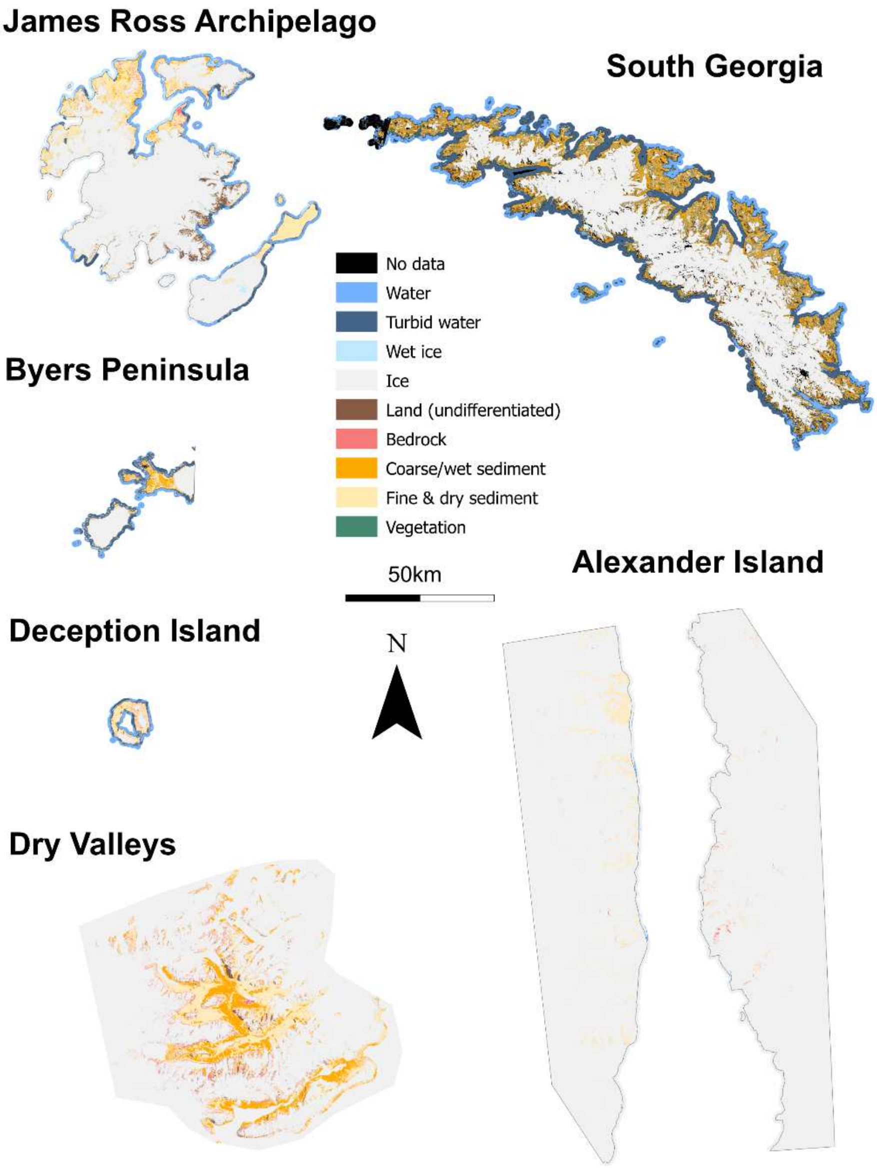

Figure 5: Land cover maps of the six sites, including 10 classes, which describe eight distinct surfaces. NB: ice class may include limited areas of seasonal snow cover. Higher resolution maps can be found in the supplementary material (Section 2).

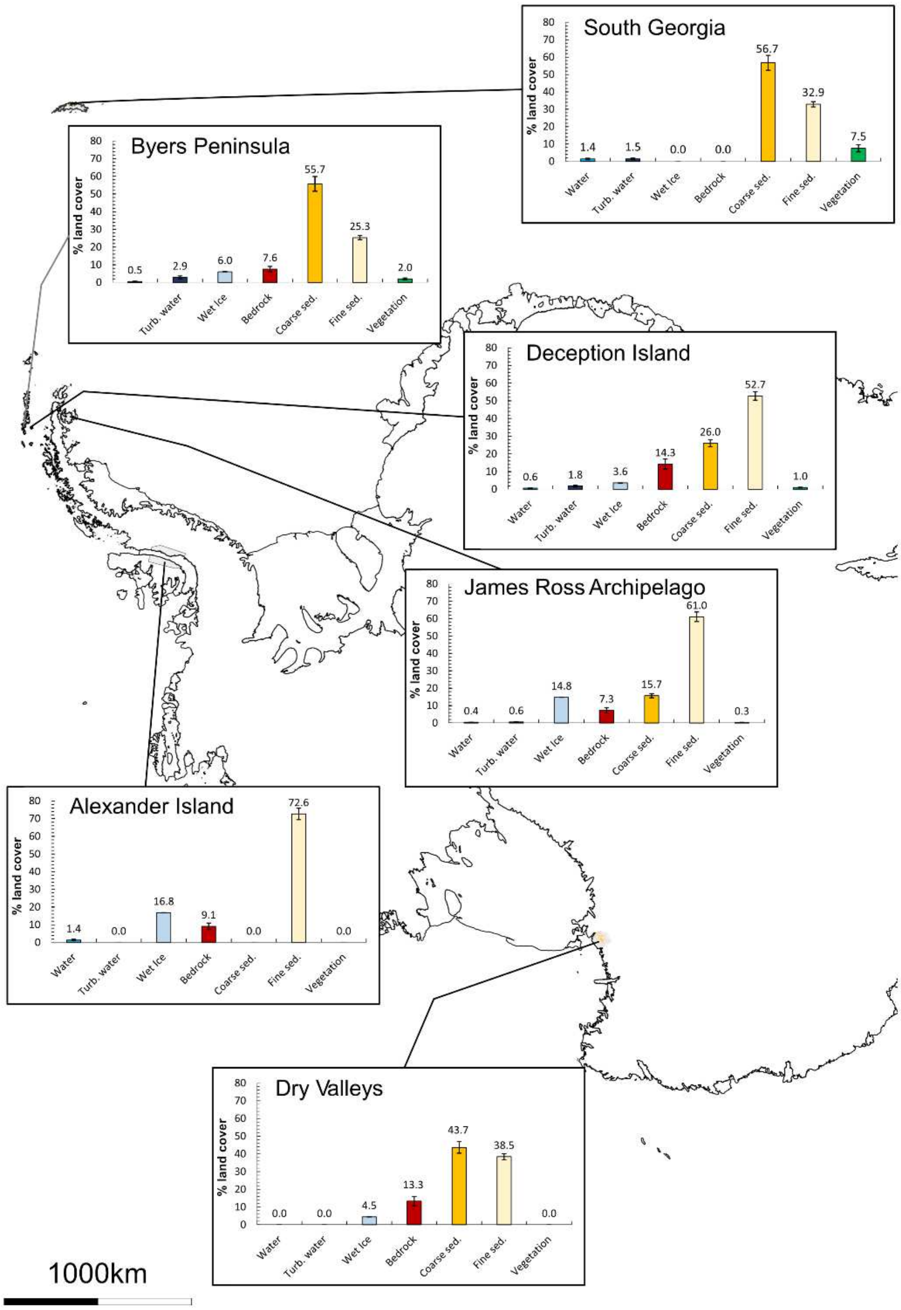

Figure 6: Percentage land cover values (excluding ice, no data and land (undifferentiated)) for each site, overlaying the coastline of Antarctica (coastline sourced from BAS). Error bars indicate the 95% confidence intervals.

The classes relating to water (water, turbid water, wet ice) are of varying quantities across all of the sites, and may represent transient features (e.g. seasonal melt water/sediment plumes). The wet-ice class proved to be a little ambiguous to interpret from clusters and represents saturated firn and 'slush' ice (i.e. partially melted ice or partially frozen water). Wet ice is most abundant on Alexander Island, with 17 % coverage (Fig. 6), and highlights the record-high surface melt observed around the King George VI Ice Shelf in late 2019 (Banwell et al., 2021). This large amount of wet ice is comparable to the James Ross Archipelago (15 %), where a large proportion of wet ice is accounted for by a melt event that resulted in a large area of saturated firn on Snow Hill Island (Fig. 7). This transient nature of wet ice is also seen with the turbid water class, which can pick out sediment plumes (Fig. 7).

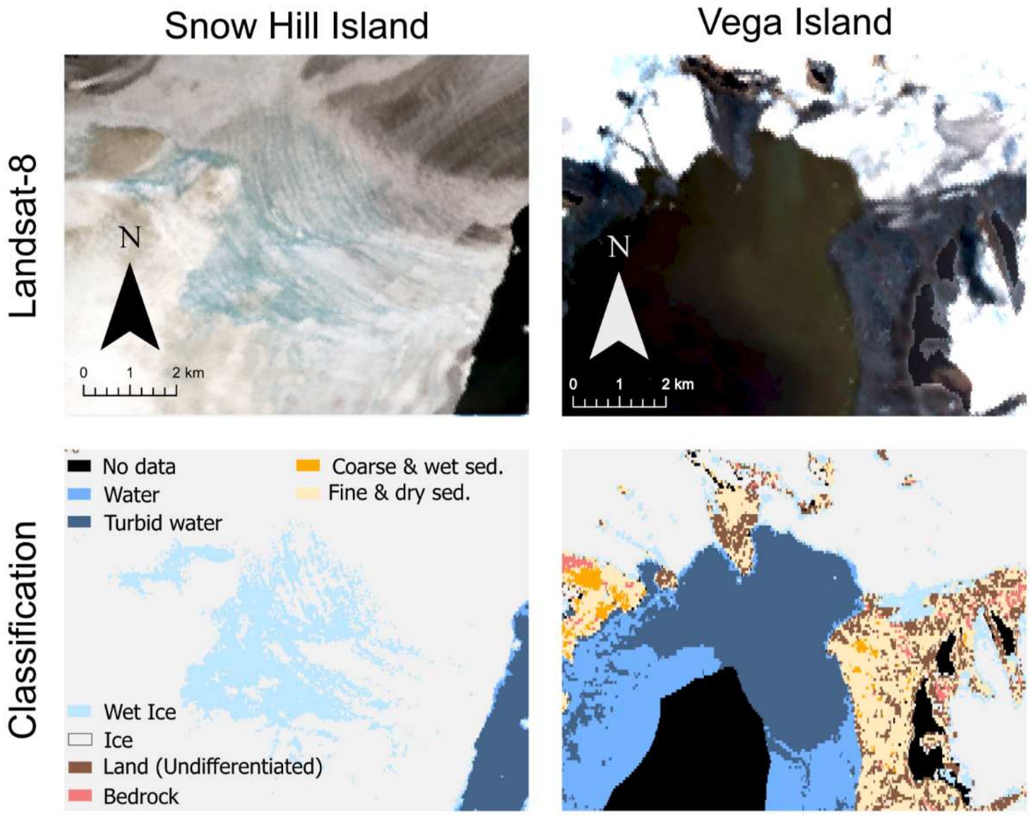

Figure 7: How the wet ice and turbid water classes compare to the images they are derived from, with a large area of saturated firn on Snow Hill Island (64°28'S, 57°4W) , and a sediment plume off the coast of Vega Island (63°52'S, 57°16'W)

Our land classification has also identified regions of vegetation. This includes extensive areas of vegetation on South Georgia, which we have calculated to cover 8 % of its proglacial surface and are clearly identifiable in satellite images (Fig. 6). We have also identified several sites of vegetation on the South Shetland Islands; especially those on Deception Island (total 1 % surface coverage, Fig. 6) within ASPA 140 (subsite B) on Deception Island (Secretariat of the Antarctic Treaty, 2022). In some cases, we have even been able to identify very small areas of vegetation such as those located on James Ross Island, which were verified in the field (Fig. 4).

3.1.2. Spatial variations

We observe a spatial variation in land cover between the sites (Fig. 5, 6). There is typically more coarse/wet sediment at sites further away from the pole; this is offset by a general decrease in fine and dry sediments. However, the Dry Valleys are an exception to this, with 44 % of the land covered by coarse or wet sediments. The second most southern site, Alexander Island, has 0 % of its proglacial surface covered by coarse/wet sediment, compared with 57 % on South Georgia.

Unlike other land classes, the proportion of the (inland) water and wet ice classes appears to be more evenly spread across the sites. There is a slight apparent latitudinal pattern in these data, with more water at the sites further to the north, and variability between the east and west (i.e. when comparing the South Shetland Islands with James Ross Archipelago, Fig. 6). South Georgia and Byers' Peninsula have the largest amount of liquid water present (when joining the water and turbid water classes together), around 3 %. James Ross Archipelago has significantly less (1 %) and Alexander Island has 1 % of its surfaces classified as water, owing to a large amount of supraglacial water at the time of image acquisition. We classified some of this melt as water, rather than wet ice, as it was unambiguously liquid when we inspected and interpreted the clusters. Much of these inter-site differences in liquid water likely represent differences in climatic setting; those sites with the greatest proportion of the water class are in milder, maritime climates, with higher temperatures and more of its precipitation falling as rain. The bedrock class does not show a clear latitudinal pattern and is most abundant in Deception Island (14 %) and the McMurdo Dry Valleys (13 %).

We noted a latitudinal pattern in the presence of vegetation, with the largest proportions of vegetation coverage observed on South Georgia and the South Shetland Islands, and no coverage on Alexander Island or the McMurdo Dry Valleys. This is consistent with observations made in Arctic regions, where regions closer to the poles have significantly less vegetation coverage (Walker et al., 2018)(Walker et al., 2018). Although no vegetation was detected on Alexander Island or in the McMurdo Dry Valleys, small areas of vegetation have previously been described (Heywood et al., 1977; Pannewitz et al., 2003), though they are typically below the resolution of our classification. The most northern site of South Georgia had significantly more vegetation than any other site (7 % of the proglacial regions are covered by vegetation, Fig. 6), while the McMurdo Dry Valleys and Alexander Island have no detectable vegetation coverage. James Ross Island has very little vegetation cover (< 1 %), while the South Shetland Islands show 2 % coverage on Byer's Peninsula and 1 % on Deception Island.

3.1.3. Potential drivers of variability

The spatial pattern in sedimentary classes are consistent with the expectation that greater runoff should occur in polar regions with higher temperatures (Syvitski, 2002). Increased runoff would result in a greater proportion of the surface being covered by the coarse/wet sediment class. However, the Dry Valleys are an exception to this, with 44 % of the land covered by coarse or wet sediments (Fig. 6). This is likely due to the high relief of the region, allowing for greater mass movement and scree formation (Kirkby and Statham, 1975; Doran et al., 2002), and consistent solar radiation during the austral summer facilitating glacier melt and, in combination with subglacial drainage, the formation of large rivers such as the Onyx River (Gooseff et al., 2011; Conovitz et al., 2013; Badgeley et al., 2017). We did not identify any coarse sediment on Alexander Island. The reasoning for this is two-fold: **i)** an apparent lack of major drainage networks, and; **ii)** the scree slopes in this region appear to be small and thin. When viewed from Sentinel-2 images, we could identify only small-size scree slopes and very few streams, consistent with observations made by (Heywood et al., 1977), who noted that many scree slopes were composed of fine sediments.

The spatial patterns in the wet ice, water and turbid water classes show more water at the sites further to the north, and variability between the east and west, likely due to climatic conditions favouring liquid water on the South Shetland Islands and South Georgia. The disproportionately large amount of water and wet ice on Alexander Island and the James Ross Archipelago relates to the high melt in these areas at the time of image acquisition (Banwell et al., 2021). The bedrock class is most abundant on Deception Island and McMurdo Dry Valleys, owing to ongoing volcanism on Deception Island (Smellie et al., 2002; Rosado et al., 2019) and extensive volcanic history of the McMurdo Dry Valleys (Petford and Mirhadizadeh, 2017;

Smellie and Martin, 2021). This class is also associated with volcanic rocks on James Ross Island (Mlčoch et al., 2020; Jennings et al., 2021), Byers Peninsula (Gao et al., 2018) and metamorphic rock outcrops on Alexander Island (British Antarctic Survey, 1981).

Whilst latitude accounts for some of the variation in vegetation coverage, it is not the only factor. The sparse vegetation coverage on James Ross Island, despite its relatively low latitude, is consistent with field observations and is logical given its semi-arid climate and high wind speeds (Martin and Peel, 1978; Davies et al., 2013; Barták et al., 2015; Nývlt et al., 2016; Hrbáček and Uxa, 2020; Kňažková et al., 2021; Váczi and Barták, 2022). The relatively high vegetation coverage of Byers Peninsula and South Georgia is also logical given the milder, maritime climates of the South Shetland Islands and South Georgia, compared to the drier continental climate of Alexander Island and the McMurdo Dry Valleys. Deception Island has less vegetation than the neighbouring Byers' Peninsula, perhaps due to the impact of ongoing volcanic activity on the island and relatively recent eruptions resulting in unfavourable conditions (Collins, 1969; Smith, 2005, 1988).

3.2. The changing landscape

Out of the five sites we investigated for change, four had similar landscape stability with between 64.2 % and 68.2 % of the land cover remaining unchanged during our study period (Fig. 8). Alexander Island, however, varies from this trend with a no change proportion of just 50.2 %. This is primarily due to the exceptional melt of snow and ice in the region at the time of the second image (2019), which led to more sediment being exposed (ITF) and some lakes and supraglacial lakes (ITT) forming in their place. 84 % of the change on Alexander Island is due to loss of the ice class, associated with snow and ice melt (a list of abbreviations can be found in **Table 2**). This dramatic change in land cover coincides with sustained positive-degree temperatures that occurred in 2019 for the contemporary image and also led to exceptional melt on the George VI ice shelf (Banwell et al., 2021).

Alexander Island is also the exception to a general pattern we observe in the loss of ice across Antarctica. In general, there is a latitudinal pattern in the loss of ice across our sites. If we consider the ITT, ITC ad ITF classes, South Georgia had 45 % of its land cover change associated with ice loss. In contrast, this value was less than 1 % for the Dry Valleys; two orders of magnitude difference. This pattern of ice loss occurs in tandem with a southward increase in the proportion of land cover change associated with sedimentary changes (FTC, CTB, or CTF). Some of these differences in sedimentary class may also be accounted for by the stabilising and moisture-retaining properties of vegetation coverage (Aalto et al., 2013; Klaar et al., 2015), which is higher at the more northerly sites (Fig. 6). If we specifically consider the FTC class, we see it is most abundant on Byers Peninsula. This is likely a product of episodic changes in the flow of streams, which would be expected in the South Shetland Islands given their high rates of precipitation (Bañón et al., 2013). Of the three sites where vegetation was identified in the land cover product, the greatest change was seen on the Byers' Peninsula; with 2 % of its total change accounted for by the CTV class, exceptional vegetation growth in the South Shetland Islands is consistent with previous findings (Torres-Mellado et al., 2011).

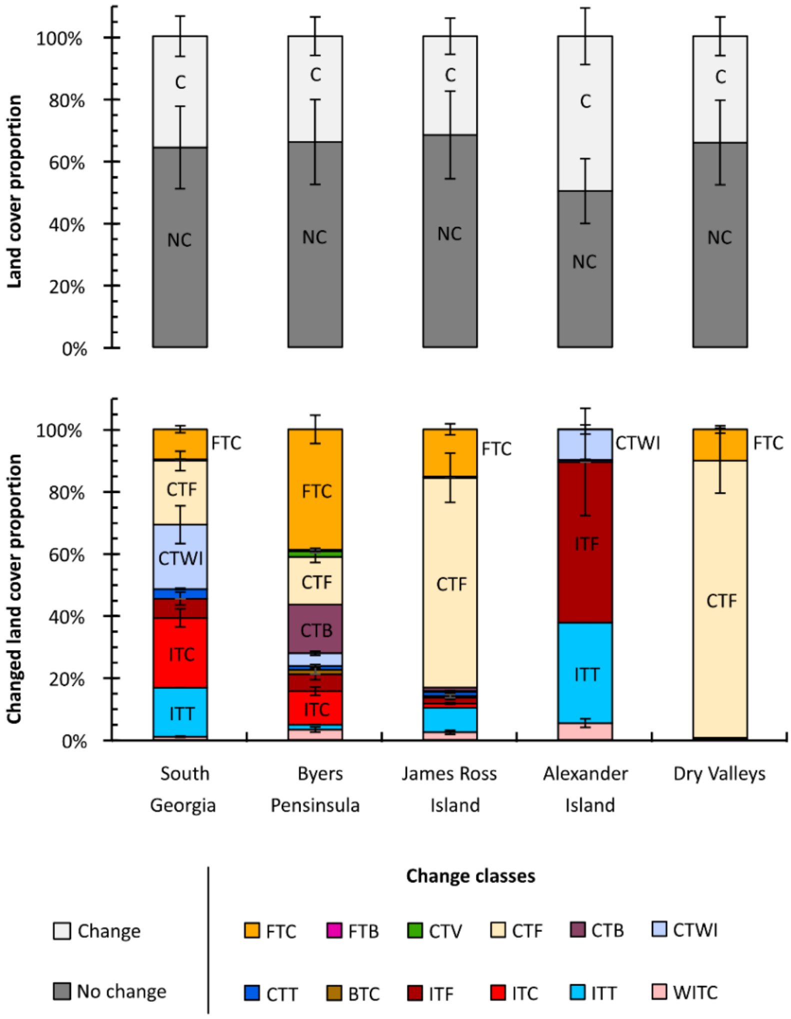

Figure 8: The proportion of the proglacial landscape that has changed at each site analysed, and the make-up of those changed regions.

3.3. Data accuracy

3.3.1. Overall accuracy of land cover product

The overall accuracy of our land cover classification is 95.9 %. However, this overall value should be taken with caution, since a large proportion of our areas of analysis are covered by ice. This high accuracy represents the fact that our approach is very effective at differentiating ice from land and water. The accuracy of each land class individually provides a more informative assessment of this approach. We find that each proglacial land class has a relatively large standard error, owing to the small number of pixels that we checked (Table 3).

Table 3: Accuracy assessment of all land classes. NB: n<3000 as several points landed on cloud-covered parts of the reference images. % error refers to the size of the 95% confidence bounds, relative to the error-adjusted area.

Class	Error-adjusted area (km^2)	95% confidence (km^2)	% Area	% error	n
Water	99.1	45.5	0.2	45.9	9
Ice	44 001.5	219.6	92.2	0.5	2 595

Bedrock	231.3	174.2	0.5	75.3	27
Fine & dry sediment	2 131.5	195.9	4.5	9.2	134
Coarse/wet sediment	1 156.6	174.2	2.4	15.1	114
Vegetation	115.7	56.4	0.2	48.8	10

The overall accuracy of the proglacial component of the classification is 77.0%, with the greatest percentage uncertainty in the smaller-sized land classes (water and vegetation). While this overall accuracy is slightly lower than some products (e.g. (Malinowski et al., 2020; Pazúr et al., 2022), it should be noted that we achieved this without the availability of extensive training data, making it more comparable with the more moderate accuracies achieved by Chen et al. (2015), for example. The sediment classes typically perform well, with relatively small percentage errors (Table 4). The confusion matrices can be found in the supplementary material (section 1.5)

Since we were unable to assess the accuracy of the turbid and wet ice classes, we have provided an example of a classification of each land class, to allow for a qualitative assessment of its accuracy (Fig. 7).

Table 4: Accuracy assessment of proglacial classes. NB: n<1000 as several points landed on cloud-covered parts of the reference images. % error refers to the size of the 95% confidence bounds, relative to the error-adjusted area.

Class	Error-adjusted area (km^2)	95% confidence (km^2)	% Area	% error	n
Water	85.7	26.4	2.0	30.9	15
Bedrock	285.5	56.7	6.6	19.9	45
Fine & dry sediment	2 375.5	106.9	54.7	4.5	371
Coarse/wet sediment	1 444.7	108.8	33.3	7.5	257
Vegetation	148.5	40.1	3.4	27.0	34

When comparing the spectra, we found that our identified classes had distinct spectral signatures that were consistent between locations (supplementary section 1.7). Some subtle differences, mostly within the red and near-infrared bands, existed in the sediment and bedrock classes, and most likely represent differences in regional geology (Salvatore et al., 2014). The pattern for vegetation is also notable. Vegetation is typically characterised by peaks in the near-infrared wavelengths; however we do not observe this in our spectra, likely because the vegetation of Antarctica is dominated by cryptogamic species (e.g. moss) which do not reflect strongly in this band (Váczi et al., 2020). The spectra for South Georgia do show a peak in the near-infrared band, consistent with the presence of vascular (leafy) vegetation (Tichit et al., 2024)

We find that our sedimentary classes are similar in spectral pattern (likely due to similarities in geology), but that the coarse/wet class present with lower reflectance values at each site (supplementary section 1.7). We interpret this to be either due to its higher water content or its higher grain size (Clark, 1990; Salvatore et al., 2023), which would explain the challenges we found in differentiating between coarse and wet sediments. We note that this distinction is not as clear with the classes on Deception Island. Whilst we have assigned K-means clusters to different classed based on the previously mapped presence of scree and streams, additional caution should be used for interpretations made at this site. The water (water and turbid water) classes are also distinct from each other (supplementary section 1.7), primarily on the basis reflectance values, consistent with previous studies showing that turbid water has higher reflectance values (Cui et al., 2022). We observed distinctly higher reflectance values for water at Alexander Island, probably because the water at this site is mostly ponded on top of glaciers/ice.

3.3.2. Spatial confidence in land cover product

We produced a map to represent the confidence of our dataset (Fig. 10), which is notable for its spatial homogeneity; no individual site appears to be more or less accurate than any other. The McMurdo Dry Valleys have the most "very low confidence" cells, but this is a function of it being the second largest site analysed, with the largest coverage of proglacial land. Since proglacial classes are less accurate than ice (Table 3 and Table 4), it is to be expected that the greatest amount of "very low confidence" cells would be present here. We also observed that many of these "very low confidence" cells contain only one or two assessment points. This means that just one inaccurate point may result in the cell being classified as "very low confidence", when in fact further analysis may reveal it performs better than is represented here.

We also note that the highest accuracy, i.e. the regions with the highest density of "very high confidence" cells, are within the ice sheets at each site, which is consistent with the analysis (Table 3). This is particularly clear on South Georgia and Alexander Island. The regions with "no points" are primarily over the large ice sheets, particularly to the centre of James Ross Island, Alexander Island and the Dry Valleys. Because of the large coverage of ice, many cells were not checked during the accuracy assessment because the random point algorithm does not regularly space points. However, in reality, we are highly confident of cells within the centre of ice sheets: they are clearly ice when inspected and the 92.4% accuracy of the ice class (Table 3) suggests they are very likely to be accurate.

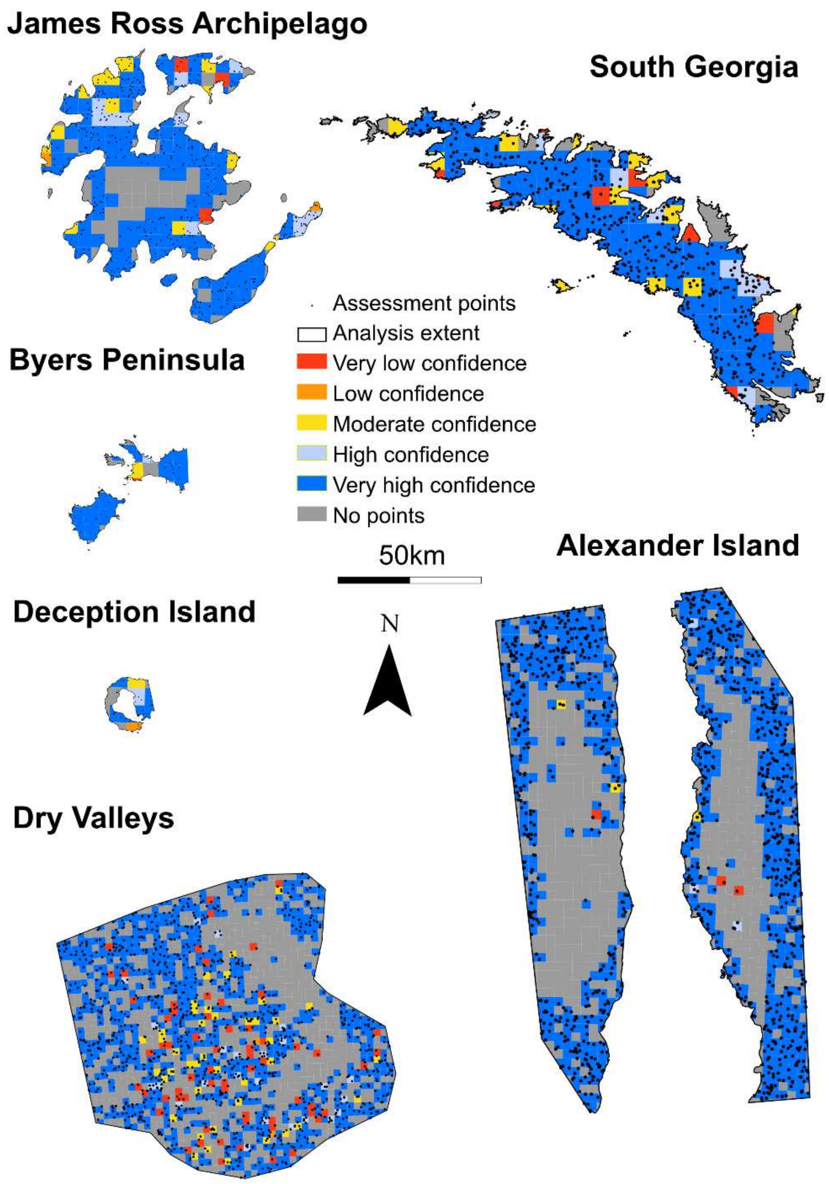

Figure 9: Maps of each site indicating the spatial variability in confidence. Very low confidence = <20% of points were accurate; low confidence = 21 to 40%; medium confidence = 41 to 60%; high confidence = 61% to 80%; very high confidence = >80%

3.3. Overall accuracy of change detection

We found our change detection approach had a total validation accuracy of 80.1 %. The accuracy varies by class (Table 5), with the most accurate class being ITT and FTB, albeit from a low sample size. The least accurate class is the Coarse/wet sediment to wet ice (CTT) class. However, as stated in section 2.4.1., it is also important to consider the geomorphological processes that the change classes represent. For example, if we merge together classes that represents the same process as CTT (i.e. formation of a lake/formation of a wet area), we see the error reduces from 60.0 % to 5.9 %.

Table 5: Accuracy assessment of land cover change. % error denotes the proportion of pixels misclassified within that land class. Geomorphological process (GP error denotes the error of the geomorphological process represented by one or more change classes.
NB: * denotes that there are two possible ways in which classes can be represented as a GP: either as lake formation and slush-ice formation, or both could be represented as one lake formation class – this affects the resultant GP error, therefore two GP errors are displayed.

Change Class	Geomorphological process (GP)	% error	GP % error	n
No change	No change	20.7	20.7	1563
Wet ice to coarse/wet sediment	Ice melt (land)	25.0	2.8	8
Ice to turbid water	Ice melt (water)	0.0	0.0	13
Ice to coarse/wet sediment	Ice melt (land)	12.7	2.8	79
Ice to fine & dry sediment	Ice melt (land)	33.3	2.8	21
Bedrock to coarse/wet sediment	Sediment deposition	6.7	6.7	15
Coarse/wet sediment to turbid water	Lake formation*	60.0	60.0/5.9	10
Coarse/wet sediment to wet ice	Slush-ice formation/ lake formation*	29.2	29.2/5.9	24
Coarse/wet sediment to bedrock	Erosion	32.3	21.6	127
Coarse/wet sediment to fine & dry sediment	Drying	15.3	15.3	98
Coarse/wet sediment to vegetation	Vegetation formation	30.8	30.8	13
Fine & dry sediment to bedrock	Erosion	0.0	21.6	1
Fine & dry sediment to coarse/wet sediment	Wetting	11.7	11.7	290

We can also visually inspect the classes of change by looking at the map of change relative to real changes in the landscape viewed from satellite images (Fig. 11). We can see that our change detection is good at detecting phase changes, such as melting ice (ITF and ITT); in the case of Alexander Island, this highlights the exposure of new sediments, while on Snow Island (Byers Peninsula site) this highlights the formation of new proglacial lakes. We are also able to detect more subtle changes in the flow of streams and the presence of wet sediments on James Ross Island (increased river activity, shown by FTC) and Seymour Island (James Ross Archipelago site) with reduced river activity and possible dust deposits.

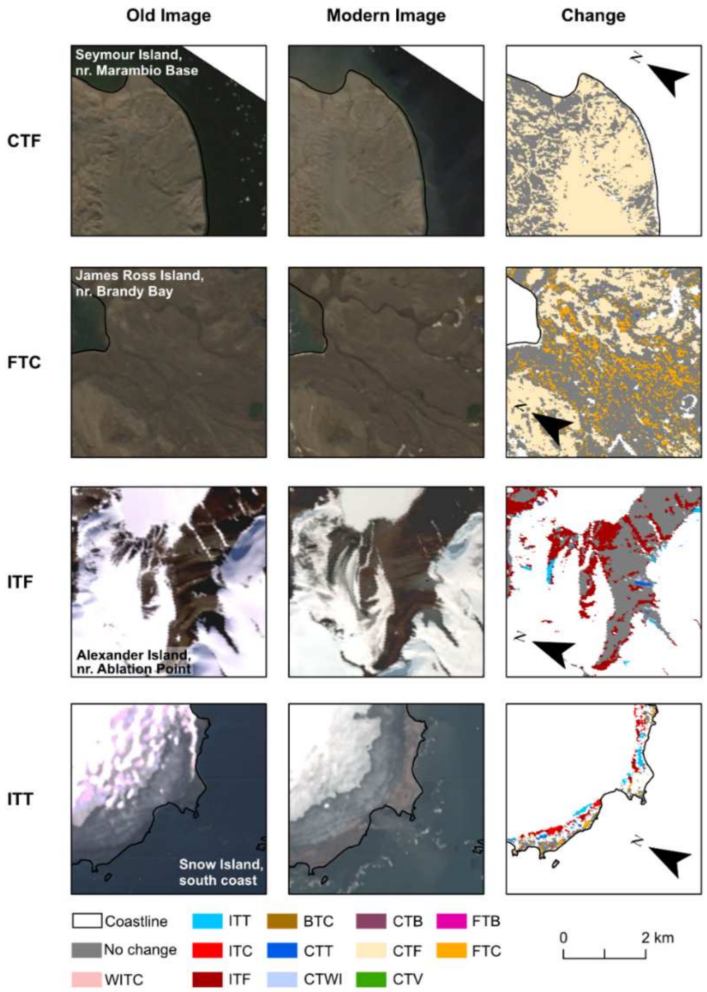

Figure 10: Examples of the four most frequently observed change classes: 86 % of the change identified in out data can be described by these four classes. The CTF example shows less active river channels in the modern image associated with drier sediments on Seymour Island. FTC shows the opposite, with more active river channels associated with wetter sediments on James Ross Island. The ITF example shows a reduction in the extent of glaciers and snowcover on Alexander Island, while the ITT example shows the development of proglacial lakes following glacier retreat on Snow Island in the South Shetland Islands. While these four panel sets are designed to highlight the four main change classes, all change classes can be seen within these panels. NB: "Modern images are derived from Landsat-8 OLI, and the old images are dervcied from Landsat-7 ETM+.

3.4. Data availability

The data used to produce these results, alongside the sampling points for the accuracy assessment and the spatial map of confidence, are available as TIFs and shapefiles at:

Stringer, C. (2022). Contemporary (2016 - 2020) land cover classification across West Antarctica and the McMurdo Dry Valleys (Version 1.0) [Data set]. NERC EDS UK Polar Data Centre. https://doi.org/10.5285/5A5EE38C-E296-48A2-85D2-E29DB66E5E24 ; and:

The land cover change maps produced from this paper are available at: Stringer, C. (2023). 21st century land cover change across the major proglacial regions of West Antarctica and the McMurdo Dry Valleys https://ramadda.data.bas.ac.uk/repository/entry/show?entryid=d6721952-a9ab-4021-adc6-1ccb4d52f1f9.

Land class spectra are available in the supplementary materials.

4. Discussion of study approach and limitations

4.1. Methodological approach

4.1.1. Landcover classification

There is a dearth of available data with which to produce an independent training data set necessary for a supervised classification approach (e.g. Random Forest Classification, Support Vector Machine) for a wide-scale land classification in Antarctica (Rodriguez-Galiano et al., 2012). Therefore, we decided to use an unsupervised classification approach. Unsupervised approaches do not require training datasets, and instead use the spectral characteristics of each pixel to statistically cluster similar pixels together without user input. The K-means algorithm is fully objective and removes the potential to target predefined classes which may be difficult to identify in medium-scale resolution satellite images, or that may be in abundance in those areas visited by mapped areas (i.e. those producing training data), but not more widely (Grimes et al., 2024). This approach is particularly useful for large, national/regional scale spatial analysis and has recently been applied to the classification of Greenland (Grimes et al., 2024; Mohd Hasmadi et al., 2009). Given land cover data are disparate and incomplete over the study sites, this approach had the added benefit that our field knowledge, as well as information from published maps of relatively small areas (Table 1) could be used to interpret clusters that cover much wider areas.

4.1.1. Change detection

There are several ways that change detection can be conducted, and these methods have previously been the subject of comprehensive literature reviews (Lu et al., 2004; Tewkesbury et al., 2015). The most commonly used of these techniques is post-classification comparisons (PCC) of image pairs. This technique involves creating a land cover classification of images in two time periods, and then directly comparing the change in classes. Although this method is intuitive, it is flawed because its overall accuracy is reliant on the accuracy of the two land cover products. Individual errors in each land cover map are compounded in the final map of change, resulting in unacceptably high uncertainty values (Lu et al., 2004; Tewkesbury et al., 2015). Change vector analysis determines the changes in the spectral properties of images over time, which allows for a classification that allows the specific type of change to be identified (Bovolo and Bruzzone, 2007). Whilst Change Vector Analysis (CVA), as used in this study, has been criticised for being difficult to interpret (Carvalho Júnior et al., 2011), recent advances in this methodology mean that the method has increased the usability of the technique, as well as its ability to identify different types of change (Xu et al., 2018). CVA determines changes in the spectral properties of images over time and has the benefit of avoiding compounding errors (Lu et al., 2004; Tewkesbury et al., 2015).

4.2. Study challenges and limitations

4.2.1. Land classification challenges

Previous studies have highlighted three key challenges when it comes to classifying terrestrial landcover: **i)** distinguishing moisture levels in soils/sediments; **ii)** distinguishing sediment grain size, and; **iii)** the spectral heterogeneity of bedrock. Whilst we have described land classes that use these terms, since they are useful geomorphological descriptors, we do not argue that we have solved these fundamental challenges associated with distinguishing between these groups spectrally, but instead address how our study has come to its final classification scheme for these groups.

In terms of moisture, our coarse/wet sediment class came from clustering of mapped features such as scree slopes and braidplains. Previous research has shown that areas of scree slope, and moisture sediments are typically associated with lower albedo values (Clark, 1990; Salvatore et al., 2023), which likely accounts for why these groups were clustered together. Nonetheless, combining these two land types in a single class provides a useful indicator of geomorphologically active regions of the landscape.

In our study we found two challenges in classifying bedrock. The first of these challenges was associated with how bedrock is typically mapped, versus how we have classified it. For example, in the Dry Valleys, bedrock accounts for 13 % of the area and the performance of the classification is particularly notable for its ability to pick out an exposed basement sill (Petford and Mirhadizadeh, 2017) in Wright Valley. In other studies (e.g. Jennings et al., 2021), bedrock classes are often over-represented (Fig. 4) because the study aims to map geomorphology or geology, rather than surface characteristics such as physical weathering and *in situ* production of block fields. Moreover, field observations show that boulders and other glacigenic sediments overlie many of the large igneous extrusions. Therefore, our classification gives a sense of mostly thin surface coverage of exposed solid bedrock. Previous work (e.g. Salvatore et al., 2014) has highlighted the spectral differences in different types of bedrock, and indeed we also found that several distinct clusters formed during our classification process that highlighted distinct igneous and metamorphic outcrops. For simplicity, these clusters were combined into a single “bedrock” class.

4.2.2 Study limitations and future work

While we made every effort to minimise the differences in the time of year between image pairs, and took further steps to ensure there was evidence of hydrological activity and minimal snow cover, there remains the possibility that some of the changes we detected are due to a differences in growing season or hydrological season, or unusual weather events. In particular, those seasonal factors could affect the area of the vegetation and coarse/wet sediment classes. Future studies should seek to ensure ground conditions are similar when conducting change detection, the first step of which is to ensure images are from as close to the same part of the hydrological and growing season as possible. Whilst it is possible to distinguish between glacial ice and snow (e.g. Awasthi and Varade, 2021; Li et al., 2022), many previous land classifications of polar regions have not done so (Grimes et al., 2024; Wang et al., 2020). Some recent studies have made use of snow masking algorithms (e.g. Roland et al., 2024), however this in itself presents a challenge in that it can alter the land area compared during change detection, which itself introduces further uncertainty. Therefore, we took the decision to follow the tried and tested approach of choosing images with limited visible snow cover.

One of the key challenges of any remote sensing study is validation, and this has been the topic of considerable discussion and review (e.g. Olofsson et al., 2013, 2014). A difficulty found in our study was the lack of existing datasets with which to validate our approach. Furthermore, those independent datasets that do exist were already exploited to aid us in the interpretation of K-means clusters (Table 1). Therefore, similar to previous research in remote regions (Grimes et al. 2024), we used our interpretations of higher resolution satellite imagery for validation. This may have introduced some biases through the misclassification of validation points, but we contend this was preferable to introducing biases from validating our approach against datasets that were used in the initial classification process. The challenges in validating this work highlight the need for further mapping of Antarctic regions based upon field observations. Alexander Island, in particular, was difficult to classify due to a lack of supporting material to aid our cluster interpretations; the most recent geological map is from 1981 (British Antarctic Survey, 1981) and only limited geomorphological maps of the region exist (Salvatore, 2001). This site highlights the need to collect more high-quality ground data in Antarctica, in order to improve our wider understanding of proglacial environments in the southernmost continent. Even projects to produce high-quality maps in small areas of these remote regions would improve the performance of remote techniques, such as those described in this study.

5. Summary and conclusions

In this study, we have created a land cover map of the major proglacial regions of sub-Antarctic islands, the Antarctic Peninsula Region, and the McMurdo Dry Valleys. Given the lack of consistent land cover or geomorphology maps in Antarctica, we used an unsupervised K-means clustering approach to classify 30 m resolution Landsat-8 OLI images by interpreting clusters in a hierarchical approach using our expert judgement and field experience in Antarctica. We present information on the coverage of nine land cover classes: turbid water, water, wet ice, ice, land (non-differentiated), bedrock, fine sediment, coarse sediment, and vegetation. We have mapped 8 distinct land surface (plus a no data and Land (undifferentiated) class) at 30 m, with an accuracy of 77.0 % for proglacial classes, and 92.2% for ice. We have also highlighted the spatial pattern in land classes, notably in vegetation and coarse/wet sediment, which are typically more abundant in sites that are more northerly. Additionally, we have analysed land cover changes in the proglacial regions of Antarctica, which we achieved using a CVA approach at an accuracy of 80.1 %. Through our analysis of change, we have highlighted a latitudinal pattern in ice loss; the proportion of landscape change on South Georgia due to the loss of ice is two orders of magnitude greater than that in the Dry Valleys. This change also occurs in tandem with the opposite pattern occurring in the sediment class changes; this is possibly also influenced by an increase in vegetation coverage in more northern sites. We have also highlighted the extensive change of the landscape that has occurred on Alexander Island where 50 % of the proglacial coverage has changed this century, likely as a consequence of recent dramatic warming events around the George VI ice shelf.

This dataset provides a first step in understanding the make-up of Antarctica's important proglacial regions. It also highlights the need for greater ground-verified data to improve the accuracy of future Antarctic land classifications. We expect that these data will further research in several disciplines, particularly those that focus on ecology, environmental sciences and atmospheric sciences, and will provide an important first dataset for monitoring environmental and ecological change in Antarctica.

Author contribution

CS produced the data, conducted the analysis and wrote the manuscript. AC supported the change detection analysis. JC conceived the project, and supported CS in writing the first draft of the manuscript. DQ and DN reviewed the manuscript prior to submission. All authors contributed to the writing.

Acknowledgements

This work is supported by the Leeds-York-Hull Natural Environment Research Council (NERC) Doctoral Training Partnership (DTP) Panorama under grant NE/S007458/1. The Ministry of Education, Youth and Sports of the Czech Republic project VAN 1/2022 and the Czech Antarctic Foundation funded fieldwork that contributed to part of this work. The Czech Antarctic Research Programme (CARP) are thanked for their support of this project, particularly for accommodating CS at the Johann Gregor Mendel Research Station on James Ross Island during the austral summer of 2021/22 and at the Nelson Island, South Shetlands facility during the austral summer of 2022/23. We also thank all of the staff at CARP for their logistical support. Michael Grimes, Elizabeth Mroz, and Eszter Kovacs of the University of Leeds and Jan Kavan of Masaryk University are thanked for their technical support. The British Antarctic Survey (BAS) and Stephen Jennings provided maps of Alexander Island and James Ross Island respectively that made this study possible. BAS also provided other resources, including aerial imagery.

Competing interests

The authors declare that they have no conflict of interest.

References

Aalto, J., le Roux, P.C. and Luoto, M. 2013. Vegetation mediates soil temperature and moisture in arctic-alpine environments. *Arctic, Antarctic, and Alpine Research*. **45**(4), pp.429–439.

Adelabu, S., Mutanga, O. and Adam, E. 2015. Testing the reliability and stability of the internal accuracy assessment of random forest for classifying tree defoliation levels using different validation methods. *Geocarto International*. **30**(7), pp.810–821.

Awasthi, S. and Varade, D. 2021. Recent advances in the remote sensing of alpine snow: a review. *GIScience & Remote Sensing*. **58**(6), pp.852–888.

Badgeley, J.A., Pettit, E.C., Carr, C.G., Tulaczyk, S., Mikucki, J.A. and Lyons, W.B. 2017. An englacial hydrologic system of brine within a cold glacier: Blood Falls, McMurdo Dry Valleys, Antarctica. *Journal of Glaciology*. **63**(239), pp.387–400.

Ballantyne, C.K. 2008. After the Ice: Holocene Geomorphic Activity in the Scottish Highlands. *Scottish Geographical Journal*. **124**(1), pp.8–52.

Ban, Y., Gong, P. and Giri, C. 2015. Global land cover mapping using Earth observation satellite data: Recent progresses and challenges. *ISPRS Journal of Photogrammetry and Remote Sensing*. **103**, pp.1–6.

Bannister, D. and King, J. 2015. Föhn winds on South Georgia and their impact on regional climate. *Weather*. **70**(11), pp.324–329.

Bañón, M., Justel, A., Velázquez, D. and Quesada, A. 2013. Regional weather survey on Byers Peninsula, Livingston Island, South Shetland Islands, Antarctica. *Antarctic Science*. **25**(2), pp.146–156.

Banwell, A.F., Tri Datta, R., Dell, R.L., Moussavi, M., Brucker, L., Picard, G., Shuman, C.A. and Stevens, L.A. 2021. The 32-year record-high surface melt in 2019/2020 on the northern George VI Ice Shelf, Antarctic Peninsula. *Cryosphere*. **15**(2), pp.909–925.

Barták, M., Váczi, P., Stachoň, Z. and Kubešová, S. 2015. Vegetation mapping of moss-dominated areas of northern part of James Ross Island (Antarctica) and a suggestion of protective measures. *Czech Polar Reports*. **5**(1), pp.75–87.

Bojinski, S., Verstraete, M., Peterson, T.C., Richter, C., Simmons, A. and Zemp, M. 2014. The Concept of Essential Climate Variables in Support of Climate Research, Applications, and Policy. *Bulletin of the American Meteorological Society*. **95**(9), pp.1431–1443.

Bovolo, F. and Bruzzone, L. 2007. A theoretical framework for unsupervised change detection based on change vector analysis in the polar domain. *IEEE Transactions on Geoscience and Remote Sensing*. **45**(1), pp.218–236.

British Antarctic Survey 1981. British Antarctic Territory geological map : scale 1:500,000 , Sheet 4 G. Britain. D. of O. Surveys, ed.

Brown, C.F., Brumby, S.P., Guzder-Williams, B., Birch, T., Hyde, S.B., Mazzariello, J., Czerwinski, W., Pasquarella, V.J., Haertel, R., Ilyushchenko, S., Schwehr, K., Weisse, M., Stolle, F., Hanson, C., Guinan, O., Moore, R. and Tait, A.M. 2022. Dynamic World, Near real-time global 10 m land use land cover mapping. *Scientific Data*. **9**(1), p.251.

Brussaard, C.P.D., Wilhelm, S.W., Thingstad, F., Weinbauer, M.G., Bratbak, G., Heldal, M., Kimmance, S.A., Middelboe, M., Nagasaki, K., Paul, J.H., Schroeder, D.C., Suttle, C.A., Vaqué, D. and Wommack, K.E. 2008. Global-scale processes with a nanoscale drive: the role of marine viruses. *The ISME Journal*. **2**(6), pp.575–578.

Burton-Johnson, A., Black, M., Fretwell, P.T. and Kaluza-Gilbert, J. 2016. An automated methodology for differentiating rock from snow, clouds and sea in Antarctica from Landsat 8 imagery: a new rock outcrop map and area estimation for the entire Antarctic continent. *The Cryosphere*. **10**(4), pp.1665–1677.

Carrasco, J.F., Bozkurt, D. and Cordero, R.R. 2021. A review of the observed air temperature in the Antarctic Peninsula. Did the warming trend come back after the early 21st hiatus? *Polar Science*. **28**, p.100653.

Carrivick, J., Heckmann, T., Fischer, M. and Davies, B. 2019. An Inventory of Proglacial Systems in Austria, Switzerland and Across Patagonia *In*: T. Heckmann and D. Morche, eds. Cham: Springer International Publishing, pp.43–57.

Carrivick, J.L., Heckmann, T., Turner, A. and Fischer, M. 2018. An assessment of landform composition and functioning with the first proglacial systems dataset of the central European Alps. *Geomorphology*. **321**, pp.117–128.

Carvalho Júnior, O.A., Guimarães, R.F., Gillespie, A.R., Silva, N.C. and Gomes, R.A.T. 2011. A new approach to change vector analysis using distance and similarity measures. *Remote Sensing*. **3**(11), pp.2473–2493.

Chasmer, L., Mahoney, C., Millard, K., Nelson, K., Peters, D., Merchant, M., Hopkinson, C., Brisco, B., Niemann, O., Montgomery, J., Devito, K. and Cobbaert, D. 2020. Remote Sensing of Boreal Wetlands

2: Methods for Evaluating Boreal Wetland Ecosystem State and Drivers of Change. *Remote Sensing*. **12**(8), p.1321.

Chen, W., Li, X. and Wang, L. 2019. Fine Land Cover Classification in an Open Pit Mining Area Using Optimized Support Vector Machine and WorldView-3 Imagery. *Remote Sensing*. **12**(1), p.82.

Chinn, T. and Mason, P. 2016. The first 25 years of the hydrology of the Onyx River, Wright Valley, Dry Valleys, Antarctica. *Polar Record*. **52**(1), pp.16–65.

Clapperton, C.M. (Chalmers M. 1971. *Geomorphology of the Stromness Bay-Cumberland Bay area, South Georgia* . London: British Antarctic Survey.

Collins, N.J. 1969. The effects of volcanic activity on the vegetation of Deception Island. *British Antarctic Survey Bulletin*. **21**, pp.79–94.

Conovitz, P.A., Mcknight, D.M., Macdonald, L.H., Fountain, A.G. and House, H.R. 2013. Hydrologic Processes Influencing Streamflow Variation in Fryxell Basin, Antarctica *In*: Ecosystem Dynamics in a Polar Desert: the McMurdo Dry Valleys, Antarctica, J.C. Priscu (Ed.)., pp.93–108.

Convey, P. and Smith, R.I.L. 2007. Responses of terrestrial Antarctic ecosystems to climate change *In*: J. Rozema, R. Aerts and H. Cornelissen, eds. *Plants and Climate Change*. Dordrecht: Springer Netherlands, pp.1–12.

Costa, A., Molnar, P., Stutenbecker, L., Bakker, M., Silva, T.A., Schlunegger, F., Lane, S.N., Loizeau, J.L. and Girardclos, S. 2018. Temperature signal in suspended sediment export from an Alpine catchment. *Hydrology and Earth System Sciences*. **22**(1), pp.509–528.

Cox, S.C., Smith Lyttle, B., Elkind, S., Smith Siddoway, C., Morin, P., Capponi, G., Abu-Alam, T., Ballinger, M., Bamber, L., Kitchener, B., Lelli, L., Mawson, J., Millikin, A., Dal Seno, N., Whitburn, L., White, T., Burton-Johnson, A., Crispini, L., Elliot, D., Elvevold, S., Goodge, J., Halpin, J., Jacobs, J., Martin, A.P., Mikhalsky, E., Morgan, F., Scadden, P., Smellie, J. and Wilson, G. 2023. A continent-wide detailed geological map dataset of Antarctica. *Scientific Data*. **10**(1).

Cui, M., Sun, Y., Huang, C. and Li, M. 2022. Water turbidity retrieval based on UAV hyperspectral remote sensing. *Water*. **14**(1), p.128.

Davies, B.J., Carrivick, J.L., Glasser, N.F., Hambrey, M.J. and Smellie, J.L. 2012. Variable glacier response to atmospheric warming, northern Antarctic Peninsula, 1988-2009. *Cryosphere*. **6**(5), pp.1031–1048.

Davies, B.J., Glasser, N.F., Carrivick, J.L., Hambrey, M.J., Smellie, J.L. and Nývlt, D. 2013. Landscape evolution and ice-sheet behaviour in a semi-arid polar environment: James Ross Island, NE Antarctic Peninsula. *Geological Society, London, Special Publications*. **381**(1), pp.353–395.

Davies, B.J., Hambrey, M.J., Glasser, N.F., Holt, T., Rodés, A., Smellie, J.L., Carrivick, J.L. and Blockley, S.P.E. 2017. Ice-dammed lateral lake and epishelf lake insights into Holocene dynamics of Marguerite Trough Ice Stream and George VI Ice Shelf, Alexander Island, Antarctic Peninsula. *Quaternary Science Reviews*. **177**, pp.189–219.

Doran, P.T., McKay, C.P., Clow, G.D., Dana, G.L., Fountain, A.G., Nylen, T. and Lyons, W.B. 2002. Valley floor climate observations from the McMurdo dry valleys, Antarctica, 1986-2000. *Journal of Geophysical Research Atmospheres*. **107**(24), p.4772.

Doran, P.T., Wharton, R.A. and Lyons, W.B. 1994. Paleolimnology of the McMurdo Dry Valleys, Antarctica. *Journal of Paleolimnology*. **10**(2), pp.85–114.

Engel, Z., Láska, K., Kavan, J. and Smolíková, J. 2023. Persistent mass loss of Triangular Glacier, James Ross Island, north-eastern Antarctic Peninsula. *Journal of Glaciology*. **69**(273), pp.27–39.

Engel, Z., Láska, K., Nývlt, D. and Stachoň, Z. 2018. Surface mass balance of small glaciers on James Ross Island, north-eastern Antarctic Peninsula, during 2009-2015. *Journal of Glaciology*. **64**(245), pp.349–361.

Farr, T.G., Rosen, P.A., Caro, E., Crippen, R., Duren, R., Hensley, S., Kobrick, M., Paller, M., Rodriguez, E., Roth, L., Seal, D., Shaffer, S., Shimada, J., Umland, J., Werner, M., Oskin, M., Burbank, D. and Alsdorf, D. 2007. The Shuttle Radar Topography Mission. *Reviews of Geophysics*. **45**(2), p.RG2004.

Friedl, M.A., Sulla-Menashe, D., Tan, B., Schneider, A., Ramankutty, N., Sibley, A. and Huang, X. 2010. MODIS Collection 5 global land cover: Algorithm refinements and characterization of new datasets. *Remote Sensing of Environment*. **114**(1), pp.168–182.

Frohn, R.C., Reif, M., Lane, C. and Autrey, B. 2009. Satellite remote sensing of isolated wetlands using object-oriented classification of Landsat-7 data. *Wetlands*. **29**(3), pp.931–941.

Galera, H., Znój, A., Chwedorzewska, K.J. and Wódkiewicz, M. 2021. Evaluation of factors influencing the eradication of annual bluegrass (Poa annua L.) from Point Thomas Oasis, King George Island, Maritime Antarctica. *Polar Biology*. **44**(12), pp.2255–2268.

Gao, L., Zhao, Y., Yang, Z., Liu, J., Liu, X., Zhang, S.H. and Pei, J. 2018. New Paleomagnetic and 40Ar/39Ar Geochronological Results for the South Shetland Islands, West Antarctica, and Their Tectonic Implications. *Journal of Geophysical Research: Solid Earth*. **123**(1), pp.4–30.

GCOS 2010. Implementation plan for the global observing system for climate in support of the UNFCCC (2010 update). , p.186.

Gerrish, L., Fretwell, P., & Cooper, P. 2021. Medium resolution vector polygons of the Antarctic coastline (Version 7.4) [Data set]. *UK Polar Data Centre, Natural Environment Research Council, UK Research & Innovation*.

Gerrish, L., Fretwell, P. and Cooper, P. 2020. High resolution vector polygons of Antarctic rock outcrop (7.3) [Data set]. *UK Polar Data Centre, Natural Environment Research Council, UK Research & Innovation*.

Gong, P., Li, X., Wang, J., Bai, Y., Chen, B., Hu, T., Liu, X., Xu, B., Yang, J., Zhang, W. and Zhou, Y. 2020. Annual maps of global artificial impervious area (GAIA) between 1985 and 2018. *Remote Sensing of Environment*. **236**, p.111510.

Gooseff, M.N., McKnight, D.M., Doran, P., Fountain, A.G. and Lyons, W.B. 2011. Hydrological Connectivity of the Landscape of the McMurdo Dry Valleys, Antarctica. *Geography Compass*. **5**(9), pp.666–681.

Grimes, M., Carrivick, J.L., Smith, M.W. and Comber, A.J. 2024a. Land cover changes across Greenland dominated by a doubling of vegetation in three decades. *Scientific Reports*. **14**(1), p.3120.

Grimes, M., Carrivick, J.L., Smith, M.W. and Comber, A.J. 2024b. Land cover changes across Greenland dominated by a doubling of vegetation in three decades. *Scientific Reports*. **14**(1), p.3120.

Harangozo, S.A., Colwell, S.R. and King, J.C. 1997. An analysis of a 34-year air temperature record from Fossil Bluff (71°S, 68°W), Antarctica. *Antarctic Science*. **9**(3), pp.355–363.

Heywood, R.B., Fuchs, V.E. and Laws, R.M. 1977. A limnological survey of the Ablation Point area, Alexander Island, Antarctica. *Philosophical Transactions of the Royal Society of London. B, Biological Sciences*. **279**(963), pp.39–54.

Howat, I.M., Porter, C., Smith, B.E., Noh, M.-J. and Morin, P. 2019. The Reference Elevation Model of Antarctica. *The Cryosphere*. **13**(2), pp.665–674.

Hrbáček, F. and Uxa, T. 2020. The evolution of a near-surface ground thermal regime and modeled active-layer thickness on James Ross Island, Eastern Antarctic Peninsula, in 2006–2016. *Permafrost and Periglacial Processes*. **31**(1), pp.141–155.

Hughes, K.A., Pescott, O.L., Peyton, J., Adriaens, T., Cottier-Cook, E.J., Key, G., Rabitsch, W., Tricarico, E., Barnes, D.K.A., Baxter, N., Belchier, M., Blake, D., Convey, P., Dawson, W., Frohlich, D., Gardiner, L.M., González-Moreno, P., James, R., Malumphy, C., Martin, S., Martinou, A.F., Minchin, D., Monaco, A., Moore, N., Morley, S.A., Ross, K., Shanklin, J., Turvey, K., Vaughan, D., Vaux, A.G.C., Werenkraut, V., Winfield, I.J. and Roy, H.E. 2020. Invasive non-native species likely to threaten biodiversity and ecosystems in the Antarctic Peninsula region. *Global Change Biology*. **26**(4), pp.2702–2716.

Humlum, O., Instanes, A. and Sollid, J.L. 2003. Permafrost in Svalbard: a review of research history, climatic background and engineering challenges. *Polar Research*. **22**(2), pp.191–215.

Jennings, S.J.A., Davies, B.J., Nývlt, D., Glasser, N.F., Engel, Z., Hrbáček, F., Carrivick, J.L., Mlčoch, B. and Hambrey, M.J. 2021. Geomorphology of Ulu Peninsula, James Ross Island, Antarctica. *Journal of Maps*. **17**(2), pp.125–139.

Kaplan Pastíriková, L., Hrbáček, F., Uxa, T. and Láska, K. 2023. Permafrost table temperature and active layer thickness variability on James Ross Island, Antarctic Peninsula, in 2004–2021. *Science of the Total Environment*. **869**, p.161690.

Kavan, J. 2021. Fluvial transport in the deglaciated Antarctic catchment–Bohemian Stream, James Ross Island. *Geografiska Annaler, Series A: Physical Geography*. **104**(1), pp.1–10.

Kavan, J., Ondruch, J., Nývlt, D., Hrbáček, F., Carrivick, J.L. and Láska, K. 2017. Seasonal hydrological and suspended sediment transport dynamics in proglacial streams, James Ross Island, Antarctica. *Geografiska Annaler: Series A, Physical Geography*. **99**(1), pp.38–55.

Kirkby, M.J. and Statham, I. 1975. Surface Stone Movement and Scree Formation. *The Journal of Geology*. **83**(3), pp.349–362.

Klaar, M.J., Kidd, C., Malone, E., Bartlett, R., Pinay, G., Chapin, F.S. and Milner, A. 2015. Vegetation succession in deglaciated landscapes: implications for sediment and landscape stability. *Earth Surface Processes and Landforms*. **40**(8), pp.1088–1100.

Kňažková, M., Nývlt, D. and Hrbáček, F. 2021. Slope processes connected with snow patches in semi-arid ice-free areas of James Ross Island, Antarctic Peninsula. *Geomorphology*. **373**, p.107479.

Lea, J.M. 2018. The Google Earth Engine Digitisation Tool (GEEDiT) and the Margin change Quantification Tool (MaQiT) – simple tools for the rapid mapping and quantification of changing Earth surface margins. *Earth Surface Dynamics*. **6**(3), pp.551–561.

Lee, J.R., Raymond, B., Bracegirdle, T.J., Chadès, I., Fuller, R.A., Shaw, J.D. and Terauds, A. 2017. Climate change drives expansion of Antarctic ice-free habitat. *Nature*. **547**(7661), pp.49–54.

Łepkowska, E. and Stachnik, Ł. 2018. Which Drivers Control the Suspended Sediment Flux in a High Arctic Glacierized Basin (Werenskioldbreen, Spitsbergen)? *Water*. **10**(10), p.1408.

Li, X., Wang, N. and Wu, Y. 2022. Automated Glacier Snow Line Altitude Calculation Method Using Landsat Series Images in the Google Earth Engine Platform. *Remote Sensing*. **14**(10), p.2377.

Lu, D., Mausel, P., Brondízio, E. and Moran, E. 2004. Change detection techniques. *International Journal of Remote Sensing*. **25**(12), pp.2365–2401.

Maat, D.S., Visser, R.J.W. and Brussaard, C.P.D. 2019. Virus removal by glacier-derived suspended fine sediment in the Arctic. *Journal of Experimental Marine Biology and Ecology*. **521**, p.151227.

Malinowski, R., Lewiński, S., Rybicki, M., Gromny, E., Jenerowicz, M., Krupiński, Michał, Nowakowski, A., Wojtkowski, C., Krupiński, Marcin, Krätzschmar, E. and Schauer, P. 2020. Automated Production of a Land Cover/Use Map of Europe Based on Sentinel-2 Imagery. *Remote Sensing*. **12**(21), p.3523.

Marchant, D.R. and Head, J.W. 2007. Antarctic dry valleys: Microclimate zonation, variable geomorphic processes, and implications for assessing climate change on Mars. *Icarus*. **192**(1), pp.187–222.

Martin, P.J. and Peel, D.A. 1978. The Spatial Distribution of 10 m Temperatures in the Antarctic Peninsula. *Journal of Glaciology*. **20**(83), pp.311–317.

Mink, S., López-Martínez, J., Maestro, A., Garrote, J., Ortega, J.A., Serrano, E., Durán, J.J. and Schmid, T. 2014. Insights into deglaciation of the largest ice-free area in the South Shetland Islands (Antarctica) from quantitative analysis of the drainage system. *Geomorphology*. **225**, pp.4–24.

Mlčoch, B., Nývlt, D. and Mixa, P. 2020. *Geological map of James Ross Island–Northern part 1: 25,000*.

Mohd Hasmadi, I., Pakhriazad, H.Z. and Shahrin, M.F. 2009. Evaluating supervised and unsupervised techniques for land cover mapping using remote sensing data. *Malaysia nJournal of Society and Space*. **5**(1), pp.1–10.

Molina-Montenegro, M.A., Carrasco-Urra, F., Rodrigo, C., Convey, P., Valladares, F. and Gianoli, E. 2012. Occurrence of the Non-Native Annual Bluegrass on the Antarctic Mainland and Its Negative Effects on Native Plants. *Conservation Biology*. **26**(4), pp.717–723.

Mulvaney, R., Abram, N.J., Hindmarsh, R.C.A., Arrowsmith, C., Fleet, L., Triest, J., Sime, L.C., Alemany, O. and Foord, S. 2012. Recent Antarctic Peninsula warming relative to Holocene climate and ice-shelf history. *Nature*. **489**(7414), pp.141–144.

Nedbalová, L., Nývlt, D., Kopáček, J., Šobr, M. and Elster, J. 2013. Freshwater lakes of Ulu Peninsula, James Ross Island, north-east Antarctic Peninsula: origin, geomorphology and physical and chemical limnology. *Antarctic Science*. **25**(3), pp.358–372.

Nývlt, D., Fišáková, M.N., Barták, M., Stachoň, Z., Pavel, V., Mlčoch, B. and Láska, K. 2016. Death age, seasonality, taphonomy and colonization of seal carcasses from Ulu Peninsula, James Ross Island, Antarctic Peninsula. *Antarctic Science*. **28**(1), pp.3–16.

Oliva, M., Antoniades, D., Giralt, S., Granados, I., Pla-Rabes, S., Toro, M., Liu, E.J., Sanjurjo, J. and Vieira, G. 2016. The Holocene deglaciation of the Byers Peninsula (Livingston Island, Antarctica) based on the dating of lake sedimentary records. *Geomorphology*. **261**, pp.89–102.

Oliva, M., Navarro, F., Hrbáček, F., Hernández, A., Nývlt, D., Pereira, P., Ruiz-Fernández, J. and Trigo, R. 2017. Recent regional climate cooling on the Antarctic Peninsula and associated impacts on the cryosphere. *Science of the Total Environment*. **580**, pp.210–223.

Olofsson, P., Foody, G.M., Herold, M., Stehman, S. V, Woodcock, C.E. and Wulder, M.A. 2014. Good practices for estimating area and assessing accuracy of land change. *Remote Sensing of Environment*. **148**, pp.42–57.

Olofsson, P., Foody, G.M., Stehman, S. V and Woodcock, C.E. 2013. Making better use of accuracy data in land change studies: Estimating accuracy and area and quantifying uncertainty using stratified estimation. *Remote Sensing of Environment*. **129**, pp.122–131.

Pannewitz, S., Green, T.G.A., Scheidegger, C., Schlensog, M. and Schroeter, B. 2003. Activity pattern of the moss Hennediella heimii (Hedw.) Zand. in the Dry Valleys, Southern Victoria Land, Antarctica during the mid-austral summer. *Polar Biology*. **26**(8), pp.545–551.

Pazúr, R., Huber, N., Weber, D., Ginzler, C. and Price, B. 2022. A national extent map of cropland and grassland for Switzerland based on Sentinel-2 data. *Earth System Science Data*. **14**(1), pp.295–305.

Petford, N. and Mirhadizadeh, S. 2017. Image-based modelling of lateral magma flow: the Basement Sill, Antarctica. *Royal Society Open Science*. **4**(5), p.161083.

Phiri, D. and Morgenroth, J. 2017. Developments in Landsat land cover classification methods: A review. *Remote Sensing*. **9**(9), p.967.

Raup, B., Racoviteanu, A., Khalsa, S.J.S., Helm, C., Armstrong, R. and Arnaud, Y. 2007. The GLIMS geospatial glacier database: A new tool for studying glacier change. *Global and Planetary Change*. **56**(1–2), pp.101–110.

Rodriguez-Galiano, V.F., Ghimire, B., Rogan, J., Chica-Olmo, M. and Rigol-Sanchez, J.P. 2012. An assessment of the effectiveness of a random forest classifier for land-cover classification. *ISPRS Journal of Photogrammetry and Remote Sensing*. **67**(1), pp.93–104.

Roman, M., Nedbalová, L., Kohler, T.J., Lirio, J.M., Coria, S.H., Kopáček, J., Vignoni, P.A., Kopalová, K., Lecomte, K.L., Elster, J. and Nývlt, D. 2019. Lacustrine systems of Clearwater Mesa (James Ross Island, north-eastern Antarctic Peninsula): geomorphological setting and limnological characterization. *Antarctic Science*. **31**(4), pp.169–188.

Rosa, K.K. da, Perondi, C., Veettil, B.K., Auger, J.D. and Simões, J.C. 2020. Contrasting responses of land-terminating glaciers to recent climate variations in King George Island, Antarctica. *Antarctic Science*. **32**(5), pp.398–407.

Rosado, B., Fernández-Ros, A., Berrocoso, M., Prates, G., Gárate, J., de Gil, A. and Geyer, A. 2019. Volcano-tectonic dynamics of Deception Island (Antarctica): 27 years of GPS observations (1991–2018). *Journal of Volcanology and Geothermal Research*. **381**, pp.57–82.

Salvatore, M.C. 2001. Geomorphological sketch map of the Fossil Bluff area (Alexander Island, Antarctica) mapped from aerial photographs. *Antarctic Science*. **13**(1), pp.75–78.

Salvatore, M.R., Barrett, J.E., Fackrell, L.E., Sokol, E.R., Levy, J.S., Kuentz, L.C., Gooseff, M.N., Adams, B.J., Power, S.N., Knightly, J.P., Matul, H.M., Szutu, B. and Doran, P.T. 2023. The Distribution of Surface Soil Moisture over Space and Time in Eastern Taylor Valley, Antarctica. *Remote Sensing*. **15**(12).

Salvatore, M.R., Mustard, J.F., Head, J.W., Marchant, D.R. and Wyatt, M.B. 2014. Characterization of spectral and geochemical variability within the Ferrar Dolerite of the McMurdo Dry Valleys, Antarctica: weathering, alteration, and magmatic processes. *Antarctic Science*. **26**(1), pp.49–68.

Secretariat of the Antarctic Treaty 2022. ASPA 140: Parts of Deception Island, South Shetland Islands.

Smellie, J.L. 2013. Geological Map of James Ross Island 1 . James Ross Island Volcanic Group. *BAS GEOMAP 2 Series, Sheet 5, British Antarctic Survey, Cambridge.*

Smellie, J.L., Lopez-Martinez Geomorphological, J., Lopez-Martinez, J., Serrano, E., Rey, J., Headland, R.K., Hernandez-Cifuentes, F., Maestro, A., Millar, I.L., Somoza, L., Thomson, J.W. and Thomson, M.R.A. 2002. *Geology and geomorphology of Deception Island*. British Antarctic Survey.

Smellie, J.L. and Martin, A.P. 2021. Chapter 5.2a Erebus Volcanic Province: volcanology. *Geological Society, London, Memoirs*. **55**(1), pp.415–446.

Smith, R.I.L. 1988. Botanical survey of Deception Island. *British Antarctic Survey Bulletin*. (80), pp.129–136.

Smith, R.I.L. 2005. The thermophilic bryoflora of Deception Island: Unique plant communities as a criterion for designating an Antarctic Specially Protected Area. *Antarctic Science*. **17**(1), pp.17–27.

Soenen, S.A., Peddle, D.R. and Coburn, C.A. 2005. SCS+C: A modified sun-canopy-sensor topographic correction in forested terrain. *IEEE Transactions on Geoscience and Remote Sensing*. **43**(9), pp.2148–2159.

Sroková, S. and Nývlt, D. 2021. Bedload geochemical and petrophysical signature of the Algal and Bohemian streams, James Ross Island, Antarctic Peninsula. *Czech Polar Reports*. **11**, pp.203–214.

Staines, K.E.H., Carrivick, J.L., Tweed, F.S., Evans, A.J., Russell, A.J., Jóhannesson, T. and Roberts, M. 2015. A multi-dimensional analysis of pro-glacial landscape change at Sólheimajökull, southern Iceland. *Earth Surface Processes and Landforms*. **40**(6), pp.809–822.

Strother, S.L., Salzmann, U., Roberts, S.J., Hodgson, D.A., Woodward, J., Van Nieuwenhuyze, W., Verleyen, E., Vyverman, W. and Moreton, S.G. 2015. Changes in Holocene climate and the intensity of Southern Hemisphere Westerly Winds based on a high-resolution palynological record from sub-Antarctic South Georgia. *The Holocene*. **25**(2), pp.263–279.

Syvitski, J.P.M. 2002. Sediment discharge variability in Arctic rivers: implications for a warmer future. *Polar Research*. **21**(2), pp.323–330.

Tejedo, P., Benayas, J., Cajiao, D., Albertos, B., Lara, F., Pertierra, L.R., Andrés-Abellán, M., Wic, C., Luciáñez, M.J., Enríquez, N., Justel, A. and Reck, G.K. 2016. Assessing environmental conditions of Antarctic footpaths to support management decisions. *Journal of Environmental Management*. **177**, pp.320–330.

Tejedo, P., Benayas, J., Cajiao, D., Leung, Y.-F., De Filippo, D. and Liggett, D. 2022. What are the real environmental impacts of Antarctic tourism? Unveiling their importance through a comprehensive meta-analysis. *Journal of Environmental Management*. **308**, p.114634.

Tewkesbury, A.P., Comber, A.J., Tate, N.J., Lamb, A. and Fisher, P.F. 2015. A critical synthesis of remotely sensed optical image change detection techniques. *Remote Sensing of Environment*. **160**, pp.1–14.

Tichit, P., Brickle, P., Newton, R.J., Convey, P. and Dawson, W. 2024. Introduced species infiltrate early stages of succession after glacial retreat on sub-Antarctic South Georgia. *NeoBiota*. **92**, pp.85–110.

Torres-Mellado, G.A., Jaña, R. and Casanova-Katny, M.A. 2011. Antarctic hairgrass expansion in the South Shetland archipelago and Antarctic Peninsula revisited. *Polar Biology*. **34**(11), pp.1679–1688.

Váczi, P. and Barták, M. 2022. Multispectral aerial monitoring of a patchy vegetation oasis composed of different vegetation classes. UAV-based study exploiting spectral reflectance indices. *Czech Polar Reports*. **12**(1), pp.131–142.

Váczi, P., Barták, M., Bednaříková, M., Hrbáček, F. and Hájek, J. 2020. Spectral properties of Antarctic and Alpine vegetation monitored by multispectral camera: Case studies from James Ross Island and Jeseníky Mts. *Czech Polar Reports*. **10**(2), pp.297–312.

Vaughan, D.G., Marshall, G.J., Connolley, W.M., Parkinson, C., Mulvaney, R., Hodgson, D.A., King, J.C., Pudsey, C.J. and Turner, J. 2003. Recent Rapid Regional Climate Warming on the Antarctic Peninsula. *Climatic Change*. **60**(3), pp.243–274.

Walker, D.A., Daniëls, F.J.A., Matveyeva, N. V, Šibík, J., Walker, M.D., Breen, A.L., Druckenmiller, L.A., Raynolds, M.K., Bültmann, H., Hennekens, S., Buchhorn, M., Epstein, H.E., Ermokhina, K., Fosaa, A.M., Heiðmarsson, S., Heim, B., Jónsdóttir, I.S., Koroleva, N., Lévesque, E., MacKenzie, W.H., Henry, G.H.R., Nilsen, L., Peet, R., Razzhivin, V., Talbot, S.S., Telyatnikov, M., Thannheiser, D., Webber, P.J. and Wirth, L.M. 2018. Circumpolar Arctic Vegetation Classification. *Phytocoenologia*. **48**(2), pp.181–201.

Walshaw, C. V., Gray, A., Fretwell, P.T., Convey, P., Davey, M.P., Johnson, J.S. and Colesie, C. 2024. A satellite-derived baseline of photosynthetic life across Antarctica. *Nature Geoscience*. **17**(8), pp.755–762.

Wang, J.A., Sulla-Menashe, D., Woodcock, C.E., Sonnentag, O., Keeling, R.F. and Friedl, M.A. 2020. Extensive land cover change across Arctic–Boreal Northwestern North America from disturbance and climate forcing. *Global Change Biology*. **26**(2), pp.807–822.

Wilkes, M.A., Carrivick, J.L., Castella, E., Ilg, C., Cauvy-Fraunié, S., Fell, S.C., Füreder, L., Huss, M., James, W., Lencioni, V., Robinson, C. and Brown, L.E. 2023. Glacier retreat reorganizes river habitats leaving refugia for Alpine invertebrate biodiversity poorly protected. *Nature Ecology and Evolution*. **7**(6), pp.841–851.

Xu, R., Lin, H., Lü, Y., Luo, Y., Ren, Y. and Comber, A. 2018. A Modified Change Vector Approach for Quantifying Land Cover Change. *Remote Sensing*. **10**(10), p.1578.

1. Methods

1.1. Choice of K-means values

To produce our land classification map, we used a K-means clustering algorithm to split each image into 75 (K value = 75) discrete clusters. Unsupervised approaches, such as K-means do not require training datasets, and instead use the structure of an image to identify spectrally homogeneous pixels, based on a user-defined number of clusters; this is particularly useful for sites with little field information (Duda and Canty, 2002; Mohd Hasmadi et al., 2009), such as those analysed in this study.

The specific K values were determined through expert judgement and represent values that minimised the chance of misclassification. Whilst others have used statistical methods, such as the 'Elbow Method', to determine the number of clusters for analysis (Syakur et al., 2018), we chose to use our expert judgement because it allowed us to find a suitable threshold to properly identify the different land cover classes as independently mapped (Table 1) and identified in the field. The K value chosen ultimately affects the accuracy of the output (Ahmed et al., 2020) and it is, therefore, essential to assess the accuracy of the final product using independent datasets. The clusters are determined using the spectral information of each image, based on 500,000 randomly selected sampling points. We assigned each of these sections a first-order class by visually inspecting the image they were derived from. In some cases, we could not easily assign a cluster a first-order class. This was usually because a cluster had conflated shadow with dark seawater. To address this, we split these clusters using a slope threshold of 3°, with pixels <3° being assigned as water. Where this process resulted in obvious misclassification we used a random forest classifier to differentiate between water, land and ice. Some pixels were covered entirely by very dark shadows or clouds and, therefore, we could not classify them; these were assigned "No data".

1.2. No data/land undifferentiated classes

The largest of these examples are on South Georgia and James Ross Island. To the northwest of South Georgia (Cape Alexandra and Bird Island), we classified a large area of land as "no data", since it was entirely obscured by thick clouds in images. Similarly, we classified the southeast of James Ross Island (the largest island in the James Ross Archipelago) as "Land (undifferentiated)". This region was covered by thin clouds in the imagery, which allowed us to differentiate land from ice and water, but it meant that we could not assign the land a second-order class with any confidence.

1.3. Use of maps to classify K-means clusters

Each map used its own nomenclature, but we found different land classes primarily centred on vegetation, bedrock outcrops, and landforms made of unlithified sedimentary rocks that are often defined by their grain size. Of the proglacial land classes, the two sedimentary classes (coarse/wet sediment and fine and dry sediment) are dominant (73 % - 90 % coverage).

1.4. Change detection

First, we merged each image pair to create an 18-band image with spectral information from both images (i.e. $Band1_{L7}$, $Band1_{L8}$, $Band2_{L7}$, $Band2_{L8}$ …). We then added three further bands to describe: **i)** the magnitude of change in reflectance intensity between the images in each image pair, as described by the Euclidian distance (ED, Eq. (4)); **ii)** the change vector direction angle (DA. Eq. (5)); and, **iii)** the spectral angle mapper (SAM, Eq. (6)).

$$ED = \sqrt{\sum_{i=1}^{n} d_i^2}\,, ED \in [0, max\,(ED)] \quad (4)$$

$$DA = \cos^{-1}\left[\frac{\sum_i^n d_i}{\sqrt{n} * ED}\right], \alpha \in [0, \pi] \quad (5)$$

$$SAM = \cos^{-1}\left[\frac{\sum_i^n Y_i * X_i}{\|Y_i\|\|X_i\|}\right] \quad (6)$$

Where:

- d_i is the difference in values for each spectral pair.
- X_i represent the spectral information of the first image
- Y_i represent the spectral information of the second image
- $\|\ \|$ represents the length of each vector

This 21-band image was then classified via a training dataset. To produce a training data set we classified the Landsat 7 image of Byers' Peninsula using the approach laid out in section 2.2.2 (i.e. K-means). We chose this site because it had the greatest variety of land classes in the contemporary classification. Across this site, we randomly selected 8,500 points and extracted the land cover at each point from both time-periods and assigned each a class-to-class (ClTCl) change value based on their land cover classification in the Landsat 7 (L7) image and Landsat 8 image (i.e. L7TL8). We removed any ClTCl changes that represented less than 1 % of the points to reduce the risk of misclassification. The remaining points described 12 ClTCl change classes (Table 2).

We then extracted band values from the 21-band image at each of these points and used them to train a random forest classifier that classified change at each site. The classifier was parameterised to have 500 trees because errors are stable around this number (Lawrence et al., 2006; Xu et al., 2018) and used to classify the 21 band image at each site. We modified the training dataset for each of our five proglacial sites to ensure that only changes between classes present in the modern land classification were possible.. As well as representing an absolute change in land cover type, change classes also describe processes. For example, the CTT class both describes a change from coarse sediment to turbid water, as well as representing a change from land to water. In the case of Alexander Island, there is no coarse sediment land cover or turbid water in either land classification. However, the CVA identified some pixels of CTT change. Therefore, we did not remove CTT as a possible change class as it accurately identified a process that was clearly visible in satellite images (i.e. ponded water where land previously was).

1.5 Confusion matrices

Confusion matrix for all land cover classes

	Reference classes									
Class	Water (1)	Ice (4)	Bedrock (6)	Coarse Sed (7)	Fine Sed (8)	Veg (9)	Total (ni)	Total area (km2)	Wi	Wi2
Water	5	3	0	0	0	1	9	91.75	2E-03	4E-06
Ice	1	2588	0	4	2	0	2595	43395.90	9E-01	8E-01
Bedrock	0	4	11	4	7	1	27	236.49	5E-03	2E-05
Coarse Sed	0	48	0	55	11	0	114	1461.23	3E-02	9E-04
Fine Sed	0	20	3	4	107	0	134	2397.77	5E-02	3E-03
Veg	0	0	0	3	2	5	10	152.66	3E-03	1E-05
Total (nj)	6	2663	14	70	129	7	2889	47735.7975		
No data	0	65	1	22	22	3				

Class	Water	Ice	Bedrock	Coarse	Fine	Veg	Totalˆ(pi)	Ûi	ˆ pj
Water	0.00	0.00	0.00	0.00	0.00	0.00	0.00	0.56	0.83
Turbid	0.00	0.90	0.00	0.00	0.00	0.00	0.90	1.00	0.97
Bedrock	0.00	0.00	0.00	0.00	0.00	0.00	0.01	0.41	0.79
Fine Sed	0.00	0.02	0.00	0.02	0.00	0.00	0.04	0.48	0.79
Coarse Sed	0.00	0.01	0.00	0.00	0.04	0.00	0.05	0.80	0.83
Veg	0.00	0.00	0.00	0.00	0.00	0.00	0.00	0.50	0.71
Totalˆ(pj)	0.00	0.92	0.00	0.02	0.04	0.00	1.00	3.74	4.92

Class	Error adjusted area	95% confidence	% Area	% error	n
Water	99	46	0.21%	45.92%	9
Ice	44,002	220	92.18%	0.50%	2,595
Bedrock	231	174	0.48%	75.32%	27
Fine Sed	2,132	196	4.47%	9.19%	134
Coarse Sed	1,157	174	2.42%	15.06%	114
Veg	116	56	0.24%	48.76%	10
Total	47,735.80				

Overall accuracy	95.92%

Confusion matrix of proglacial classes

	Reference classes									
Class	Water (1)	Ice (4)	Bedrock (6)	Coarse Sed (7)	Fine Sed (8)	Veg (9)	Total (ni)	Total area (km^2)	Wi	Wi2
Water	11	0	0	1	2	1	15	91.75	0.02	0.00
Ice	2	0	3	16	16	1	38	0.00	0.00	0.00
Bedrock	0	0	30	12	3	0	45	236.49	0.05	0.00
Coarse Sed	2	0	14	190	51	0	257	1461.23	0.34	0.11
Fine Sed	0	0	3	28	335	5	371	2397.77	0.55	0.31
Veg	0	0	0	6	9	19	34	152.66	0.04	0.00
Total (nj)	15	0	50	253	416	26	760	4339.899		
No data	7		5	84	197	10				

Class	Water	Ice	Bedrock	Coarse	Fine	Veg	Totalˆ(pi)	Ûi	ˆ pj
Water	0.01	0.00	0.00	0.00	0.00	0.00	0.02	0.73	0.73
Ice	0.00	0.00	0.00	0.02	0.02	0.00	0.05	0.00	0.00
Bedrock	0.00	0.00	0.04	0.02	0.00	0.00	0.06	0.67	0.60
Fine Sed	0.00	0.00	0.02	0.25	0.07	0.00	0.34	0.74	0.75
Coarse Sed	0.00	0.00	0.00	0.04	0.44	0.01	0.49	0.90	0.81
Veg	0.00	0.00	0.00	0.01	0.01	0.03	0.04	0.56	0.73
Totalˆ(pj)	0.02	0.00	0.07	0.33	0.55	0.03	1.00	3.60	3.62

Class	Error adjusted area km^2)	95% confidence	% Area	% error	n
Water	86	26	1.97%	30.87%	15
Bedrock	286	57	6.58%	19.86%	45
Fine Sed	2,376	107	54.74%	4.50%	371
Coarse Sed	1,445	109	33.29%	7.53%	257
Veg	148	40	3.42%	26.99%	34
Total	4,340				

Overall accuracy	76.97%

1.6 Images used during the analysis, including the date of image acquisition and overall cloud cover

Landsat 8 image	Date	Cloud cover %	Landsat 7 image	Date	Cloud cover %
James Ross Island					
LANDSAT/LC08/C02/T2_TOA/LC08_215105_20170204 LANDSAT/LC08/C02/T2_TOA/LC08_215105_20160202	04/02/2017 02/02/2016	6 6	LANDSAT/LE07/C02/T2_TOA/LE07_216105_20000221	21/02/2000	15
Dry Valleys					
LANDSAT/LC08/C02/T2_TOA/LC08_056116_20191217	17/12/2019	0	LANDSAT/LE07/C02/T2_TOA/LE07_059115_20011228	28/12/2000	1
Alexander Island					

LANDSAT/LC08/C02/T2_TOA/LC08_218110_20200117 LANDSAT/LC08/C02/T2_TOA/LC08_217111_20191107 LANDSAT/LC08/C02/T2_TOA/LC08_216110_20191218	17/01/2020 07/11/2019 18/12/2019	0 1 0	LANDSAT/LE07/C02/T2_TOA/LE07_213111_20020104 LANDSAT/LE07/C02/T2_TOA/LE07_217111_20021202 LANDSAT/LE07/C02/T2_TOA/LE07_218110_20010104 LANDSAT/LE07/C02/T2_TOA/LE07_218111_20030211 LANDSAT/LE07/C02/T2_TOA/LE07_214110_20030130 LANDSAT/LE07/C02/T2_TOA/LE07_218110_20030211 LANDSAT/LE07/C02/T2_TOA/LE07_219109_20011229 LANDSAT/LE07/C02/T2_TOA/LE07_132133_20001123 LANDSAT/LE07/C02/T2_TOA/LE07_216111_20030112 LANDSAT/LE07/C02/T2_TOA/LE07_217111_20010214 LANDSAT/LE07/C02/T2_TOA/LE07_214110_20020127 LANDSAT/LE07/C02/T2_TOA/LE07_217110_20021202 LANDSAT/LE07/C02/T2_TOA/LE07_218111_20010104	04/01/2002 02/12/2002 04/01/2001 11/02/2003 30/01/2003 11/02/2003 29/12/2001 23/11/2000 12/01/2003	1 1 1 1 2 2 2 3 3 3 4 4 4

				14/02/2001 27/01/2002 02/12/2002 04/01/2001	
Deception Island					
LANDSAT/LC08/C02/T2_TOA/LC08_219104_20200209	09/02/2020	21			
Byers Peninsula					
LANDSAT/LC08/C02/T2_TOA/LC08_219104_20200209	09/02/2020	21	LANDSAT/LE07/C02/T2_TOA/LE07_219104_20020130	30/01/2002	17
South Georgia					
LANDSAT/LC08/C02/T1_TOA/LC08_206098_20180328	28/03/2018 04/04/2018	2 47	LANDSAT/LE07/C02/T1_TOA/LE07_206098_20020103 LANDSAT/LE07/C02/T1_TOA/LE07_206098_20030207	03/01/2002	65 17

LANDSAT/LC08/C02/T1_TOA/LC08_207098_20180404				07/02/2003	

Images used in accuracy assessment

Accuracy assessment was conducted using Sentinel-2 MSI images that coincided with the date of image acquisition of the Landsat-8 OLI images used for the land class classification. Images with low-cloud images preferentially chosen. The code to collate these images, as well as list of images (in the console) can be found here: https://code.earthengine.google.com/6bc925765ad1a42d193d2ef43930f483 . NB: image availability was prioritised over cloud-free images. Any validation point located over cloud cover was discounted from the final accuracy assessment.

1.7 Mean spectra

Spectra:

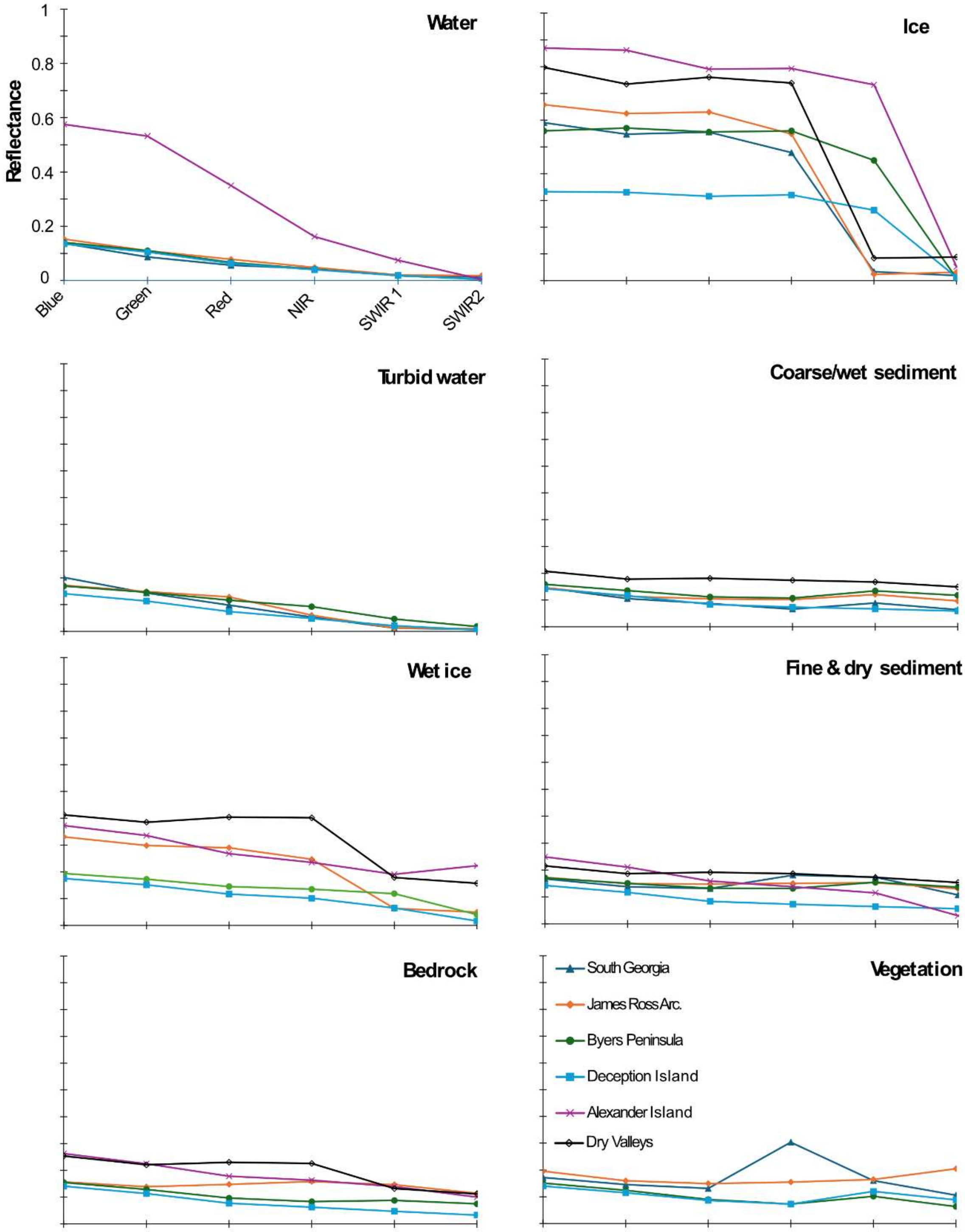

Comparisons:

NB: dotted line = coarse/turbid

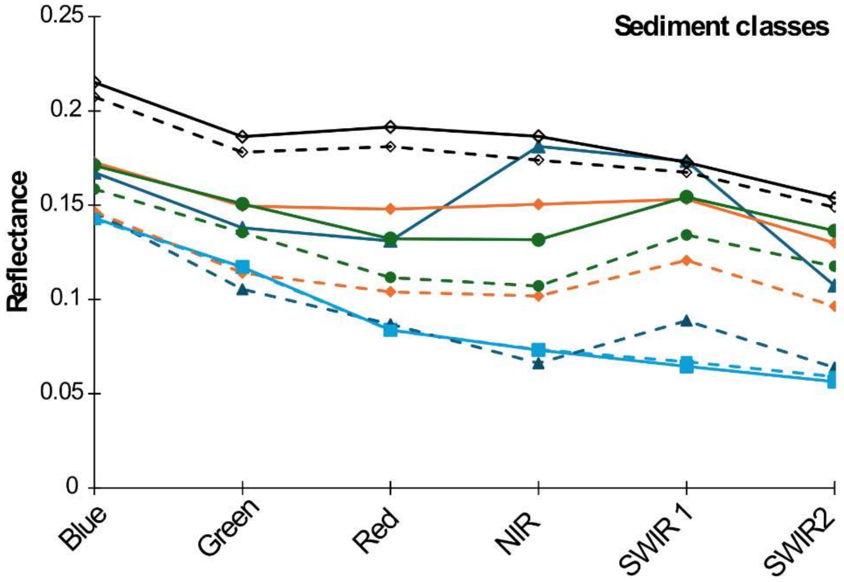

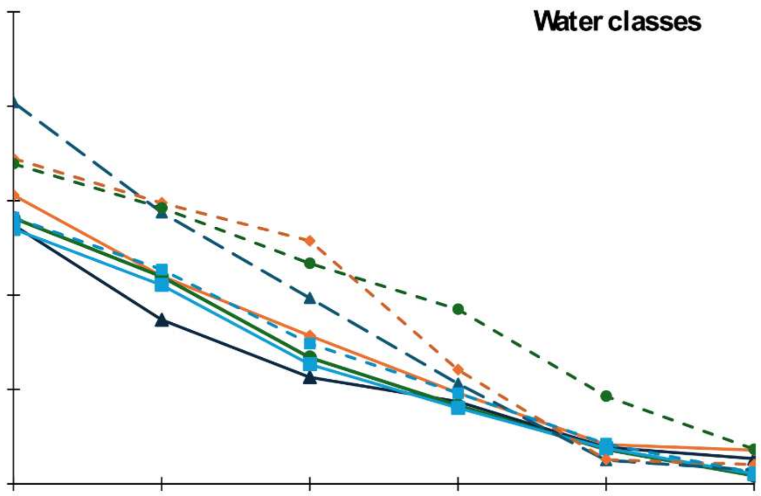

2. Land classification maps

South Georgia

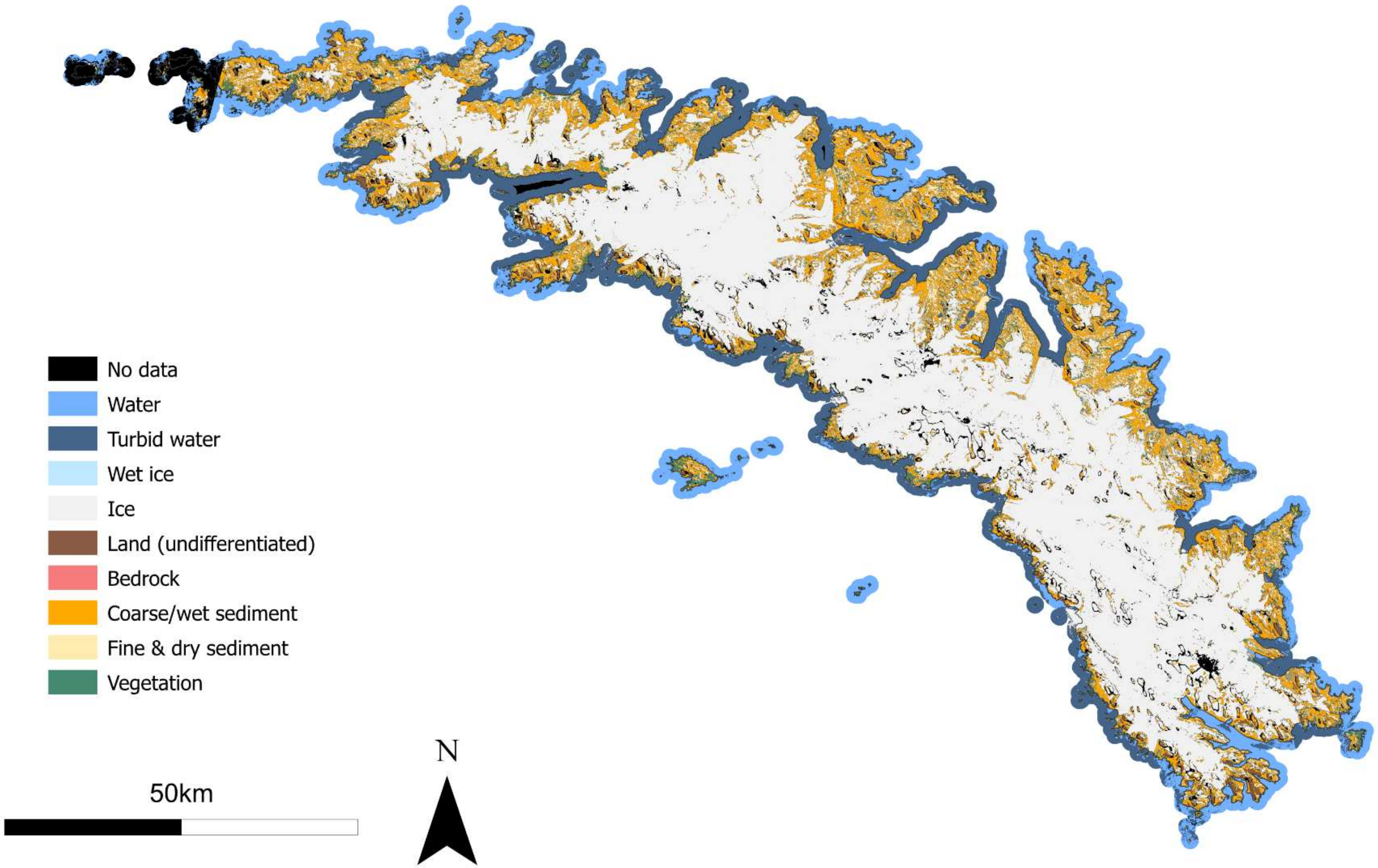

James Ross Archipelago

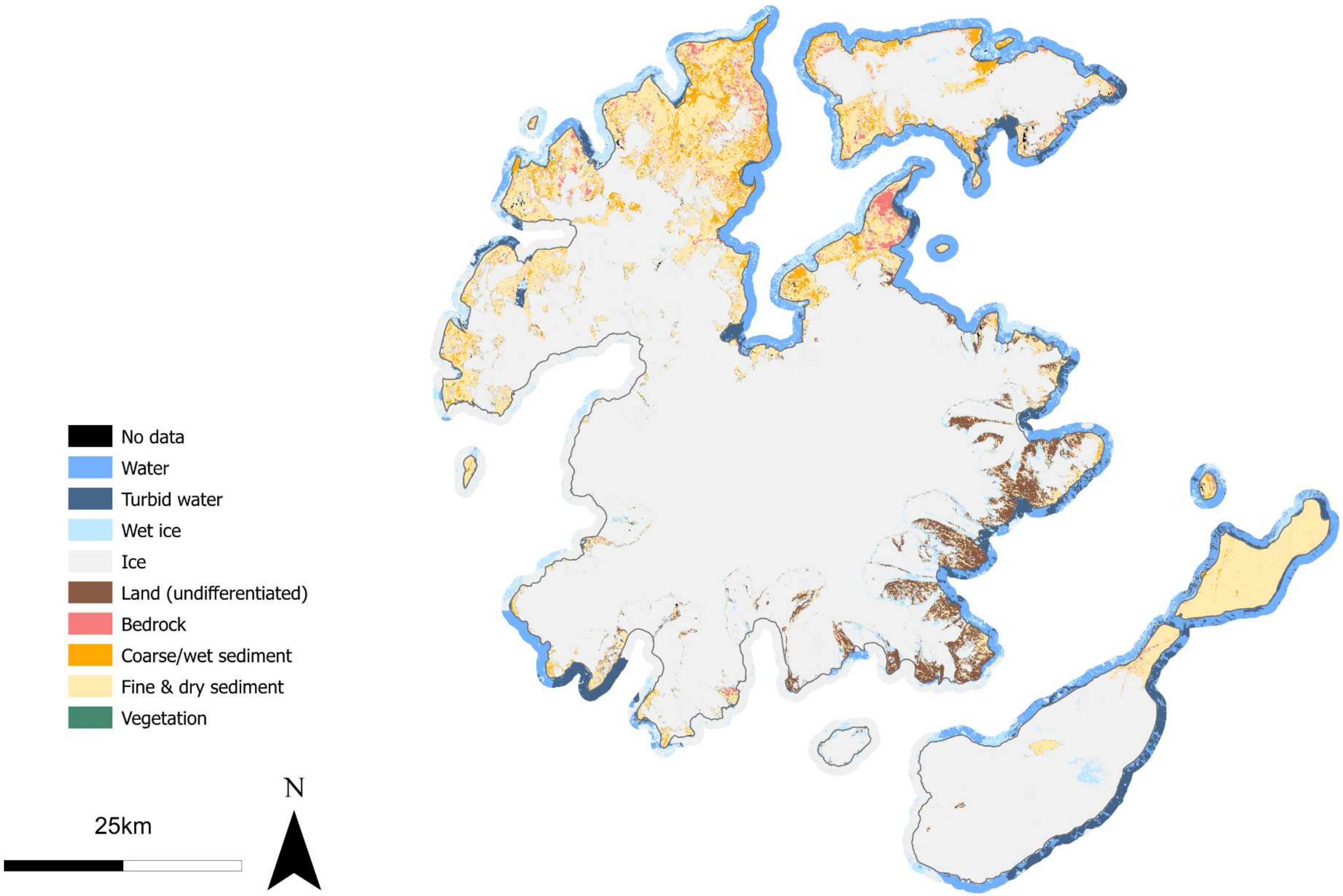

Byers Peninsula

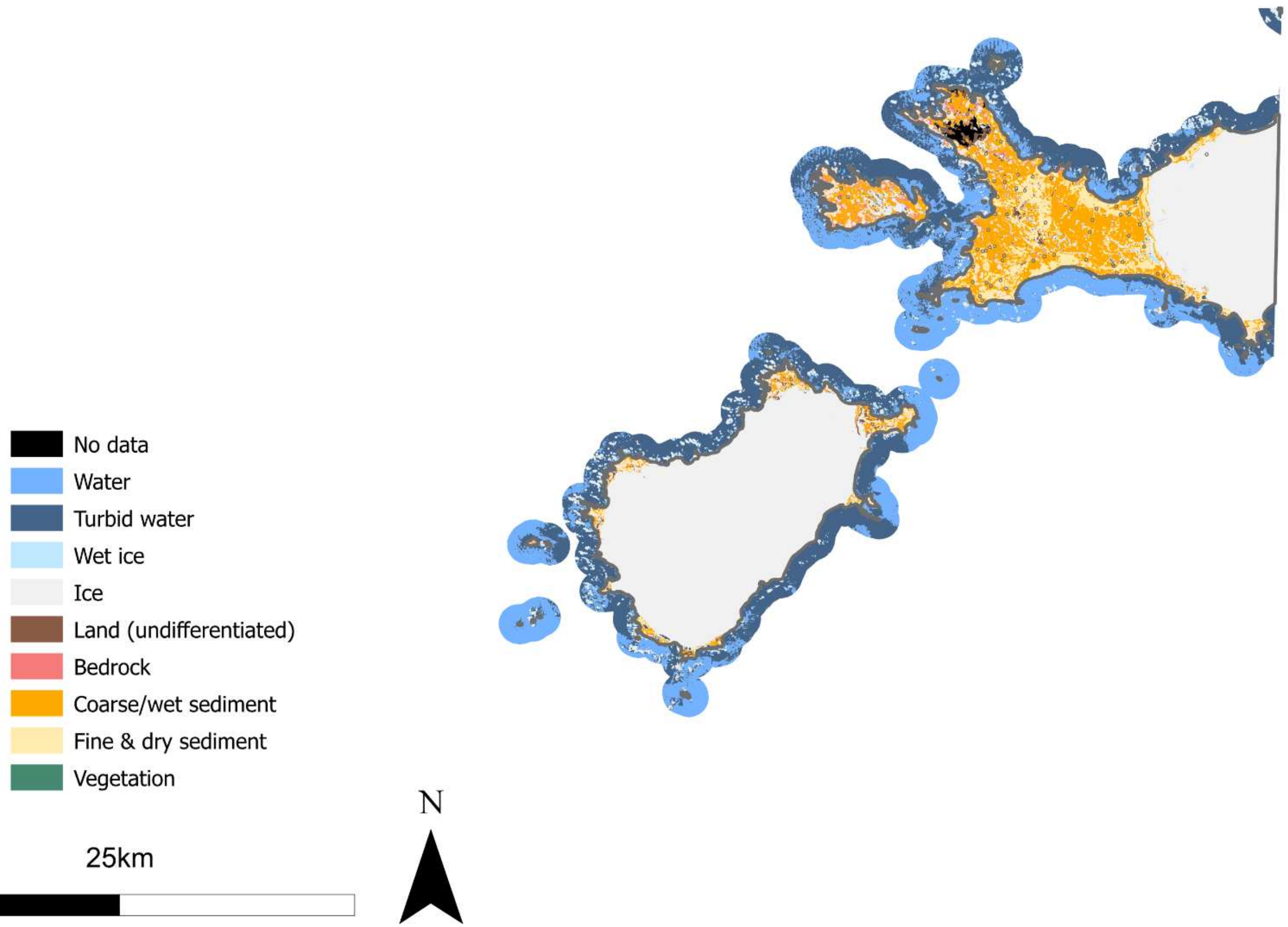

Deception Island

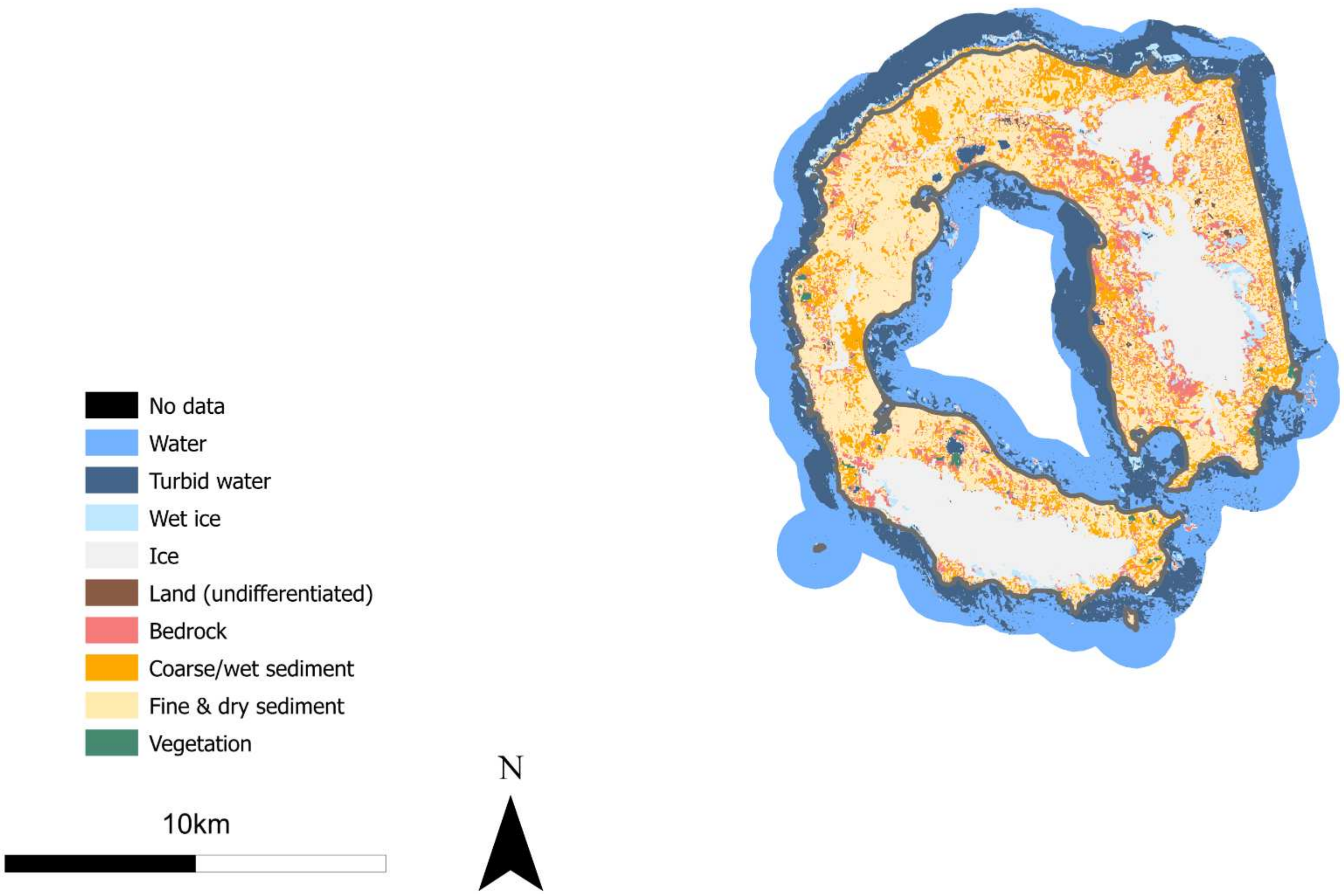

Alexander Island

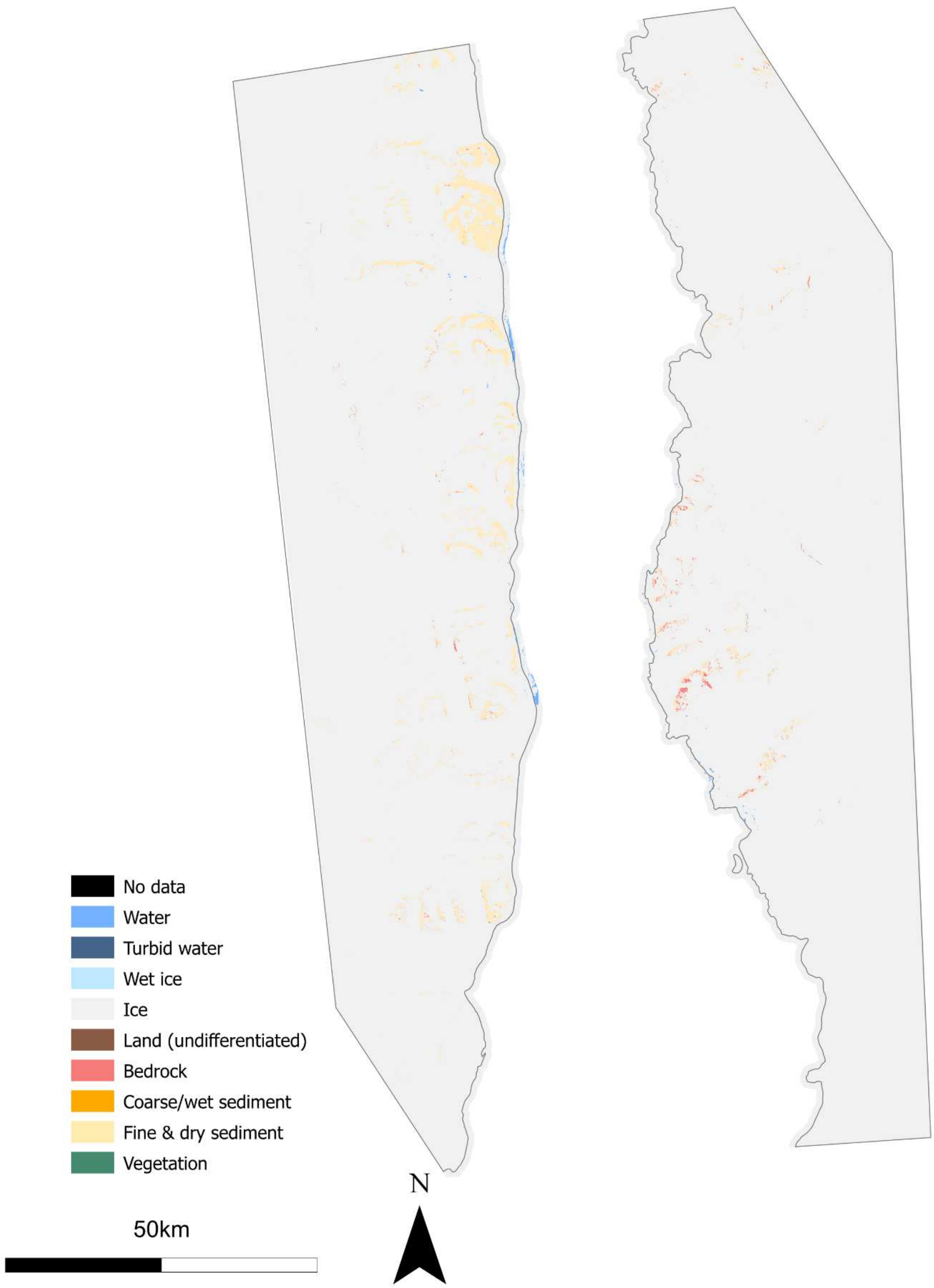

Dry Valleys

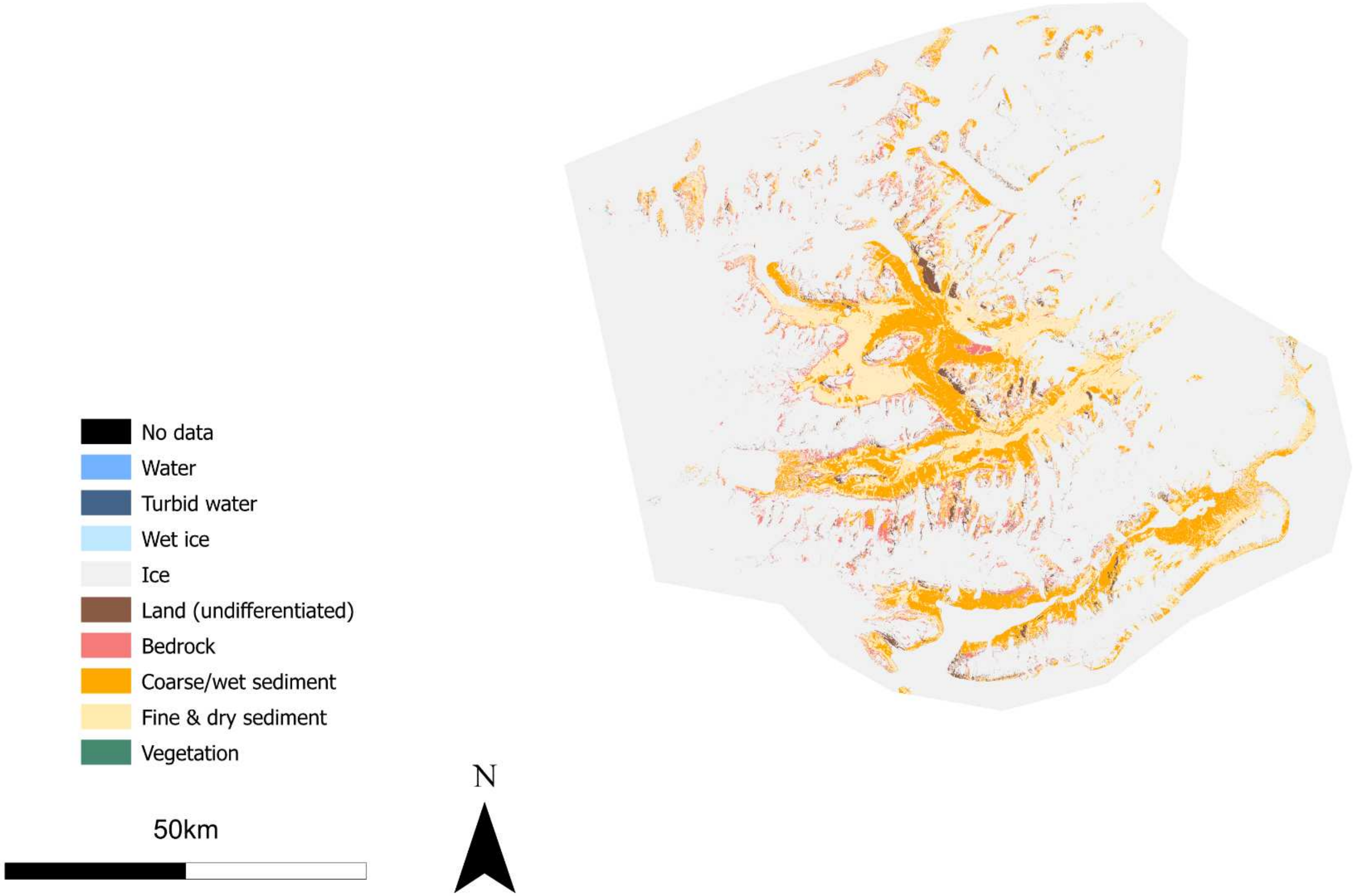

No data
Water
Turbid water
Wet ice
Ice
Land (undifferentiated)
Bedrock
Coarse/wet sediment
Fine & dry sediment
Vegetation
50km
N

References

Ahmed, M., Seraj, R. and Islam, S.M.S. 2020. The k-means algorithm: A comprehensive survey and performance evaluation. *Electronics (Switzerland)*. **9**(8), pp.1–12.

Duda, T. and Canty, M. 2002. Unsupervised classification of satellite imagery: Choosing a good algorithm. *International Journal of Remote Sensing*. **23**(11), pp.2193–2212.

Mohd Hasmadi, I., Pakhriazad, H.Z. and Shahrin, M.F. 2009. Evaluating supervised and unsupervised techniques for land cover mapping using remote sensing data. *Malaysia nJournal of Society and Space*. **5**(1), pp.1–10.

Syakur, M.A., Khotimah, B.K., Rochman, E.M.S. and Satoto, B.D. 2018. Integration K-Means Clustering Method and Elbow Method For Identification of The Best Customer Profile Cluster. *IOP Conference Series: Materials Science and Engineering*. **336**(1), p.12017.

	Water					
Region	blue	green	red	nir	swir1	swir2
SG	0.13704	0.086862	0.056441	0.04354	0.019376	0.013345
JRI	0.152812	0.110064	0.078367	0.048222	0.020767	0.017871
BP	0.140738	0.109761	0.066844	0.041494	0.018244	0.004329
DI	0.134944	0.105298	0.063254	0.04017	0.018877	0.005201
AI	0.575288	0.532354	0.350095	0.162037	0.074789	0.004446
DV						

	Turbid					
Region	blue	green	red	nir	swir1	swir2
SG	0.201999	0.143707	0.098399	0.053077	0.012557	0.007318
JRI	0.172237	0.148793	0.128677	0.060458	0.012892	0.010266
BP	0.169474	0.146118	0.116789	0.092441	0.046417	0.01833
DI	0.14101	0.113508	0.074265	0.048057	0.02126	0.005916
AI						
DV						

	Wet Ice					
Region	blue	green	red	nir	swir1	swir2
SG						
JRI	0.330555	0.298386	0.289983	0.246736	0.063194	0.049305
BP	0.193893	0.172299	0.145195	0.135257	0.118506	0.040388
DI	0.175027	0.151391	0.11682	0.101581	0.064914	0.016403
AI	0.372704	0.33559	0.267855	0.235339	0.190599	0.222842
DV	0.412788	0.38517	0.404316	0.401682	0.178636	0.157122

	Ice					
Region	blue	green	red	nir	swir1	swir2
SG	0.590638	0.547771	0.555629	0.478651	0.03359	0.019005
JRI	0.657738	0.624866	0.63022	0.548382	0.023818	0.031615
BP	0.559984	0.570724	0.555912	0.560019	0.4496	0.009149
DI	0.33295	0.330545	0.315363	0.320545	0.263397	0.012669
AI	0.869529	0.861654	0.791099	0.793005	0.732279	0.051624
DV	0.797303	0.735013	0.760796	0.738944	0.084212	0.088127

	Bedrock					
Region	blue	green	red	nir	swir1	swir2
SG						
JRI	0.156913	0.138707	0.147702	0.158231	0.14662	0.114591
BP	0.154448	0.128793	0.096384	0.083144	0.087845	0.075143
DI	0.140673	0.113257	0.076984	0.062519	0.04727	0.033018
AI	0.262669	0.22449	0.177962	0.163305	0.139424	0.099994
DV	0.253559	0.220653	0.230089	0.225743	0.132087	0.112062

	Coarse					
Region	blue	green	red	nir	swir1	swir2
SG	0.146383	0.105372	0.086826	0.066113	0.088711	0.063808
JRI	0.146692	0.114031	0.104044	0.101774	0.120692	0.096378
BP	0.158519	0.135498	0.111599	0.107118	0.134188	0.117578

DI	0.142661	0.116641	0.083653	0.073418	0.066911	0.059048
AI						
DV	0.207432	0.178076	0.181037	0.173922	0.167391	0.148944

	Fine					
Region	blue	green	red	nir	swir1	swir2
SG	0.167279	0.137951	0.131029	0.181177	0.173406	0.107326
JRI	0.172702	0.14952	0.147935	0.150416	0.153192	0.13002
BP	0.17106	0.150705	0.132187	0.131646	0.154384	0.136386
DI	0.14311	0.117158	0.083822	0.073154	0.064464	0.056382
AI	0.248993	0.210855	0.159091	0.137949	0.115097	0.030403
DV	0.215206	0.186343	0.191474	0.186543	0.172785	0.153765

	Vegetation					
Region	blue	green	red	nir	swir1	swir2
SG	0.172099	0.145411	0.131129	0.303571	0.16034	0.105848
JRI	0.195461	0.159675	0.149284	0.154674	0.164552	0.204832
BP	0.151218	0.124182	0.089762	0.072748	0.101687	0.063436
DI	0.140066	0.114645	0.086451	0.072654	0.119967	0.088167
AI						
DV						

MeanFine	0.186392	0.158755	0.140923	0.143481	0.138888	0.10238	
MeanCoarse	0.160337	0.129924	0.113432	0.104469	0.115579	0.097151	
StdevFine	0.035143	0.031061	0.032582	0.037506	0.038493	0.0445	
StdevCoarse	0.024144	0.026006	0.035374	0.03814	0.035064	0.033657	
MeanWater	0.141383	0.102996	0.066227	0.043356	0.019316	0.010186	Exc AI
MeanTurbid	0.17118	0.138032	0.104533	0.063508	0.023282	0.010458	
StdevWater	0.006917	0.009504	0.007943	0.003055	0.000929	0.005661	
StdevTurbid	0.021587	0.014272	0.020536	0.017277	0.013805	0.004809	

b1	b2	b3	b4	b5	b6